

Seasonal and Diurnal Variations in Long-Period Noise at SPREE Stations: The Influence of Soil Characteristics on Shallow Stations' Performance

by Emily Wolin, Suzan van der Lee, Trevor A. Bollmann, Douglas A. Wiens, Justin Revenaugh, Fiona A. Darbyshire, Andrew W. Frederiksen, Seth Stein, and Michael E. Wysession

Abstract The Superior Province Rifting Earthscope Experiment (SPREE) recorded continuous seismic data over the Midcontinent Rift from April 2011 through October 2013. Analysis of power spectral density (PSD) estimates shows that horizontal noise levels at periods > 20 s vary seasonally and diurnally. During winter, horizontal noise power at many SPREE stations is within 5 dB of nearby Transportable Array (TA) stations. As the ground thaws, SPREE stations in fine-grained material such as silt or clay become noisier due to changes in the mechanical properties of the soil. During summer, the daily mean PSD value of stations in fine-grained material is approximately 10–20 dB higher than in the winter, and daytime noise levels are 20–30 dB higher than nights. Stations in sandy material also show diurnal variations of 20–30 dB during summer, but the daily mean PSD value varies no more than 5–10 dB during the year. Most neighboring TA stations have relatively constant daily mean PSDs, and their horizontal components show summer diurnal variations of 10–15 dB. Some very quiet TA stations, such as SPMN, show a 5–10 dB increase in horizontal noise power during winter. The timing and amplitude of horizontal noise power variations between 20 and 800 s correlate with variations in atmospheric pressure PSDs. We propose that the grain size and pore water content of the material surrounding a shallow seismic station influences the local response to atmospheric pressure. Stations that must be placed in soft sediments should be installed in sandy, well-drained material to minimize long-period noise generated by atmospheric pressure variations.

Online Material: Figures with examples of signals, power spectra, and their differences.

Introduction

The Superior Province Rifting Earthscope Experiment (SPREE) (Van der Lee *et al.*, 2013) was installed over and around the Midcontinent Rift system in Minnesota, Wisconsin, and Ontario. This experiment was designed to image the crust and mantle below the 1.1 Ga failed rift system and investigate whether any signature remains in the now-stable continental lithosphere and surrounding stable Archean and Proterozoic lithosphere (Whitmeyer and Karlstrom, 2007; Stein *et al.*, 2011).

The geometry of the SPREE array reflects the crustal structure of the Midcontinent Rift. Sixteen stations in Ontario (SC01–SC16) expand the EarthScope Transportable Array (TA)-style coverage to the north of the rift. One line of stations (SM17–SM42) follows the gravity high along the center of the rift; another line crosses the widest portion of the gravity

anomaly (SN43–SN63); and a final line crosses the narrowest portion of the gravity anomaly (SS64–SS83) (Fig. 1).

Earthquake-based methods such as receiver functions, surface-wave dispersion measurements, full-waveform fitting, and body- and surface-wave tomography rely on signals created by regional and teleseismic events, which span a broad range of periods (generally 1–100 s). Ambient earth noise, typically between periods of 5–40 s, also has been successfully used as a signal to image Earth structure (e.g., Shapiro *et al.*, 2005, and others). Its utility lies in the fact that coherent noise between two seismic stations senses the elastic properties of the Earth between them. In contrast, site-specific phenomena or instabilities in a station's installation can produce noise that is recorded only locally and does not contain useful information about crust or mantle structure.

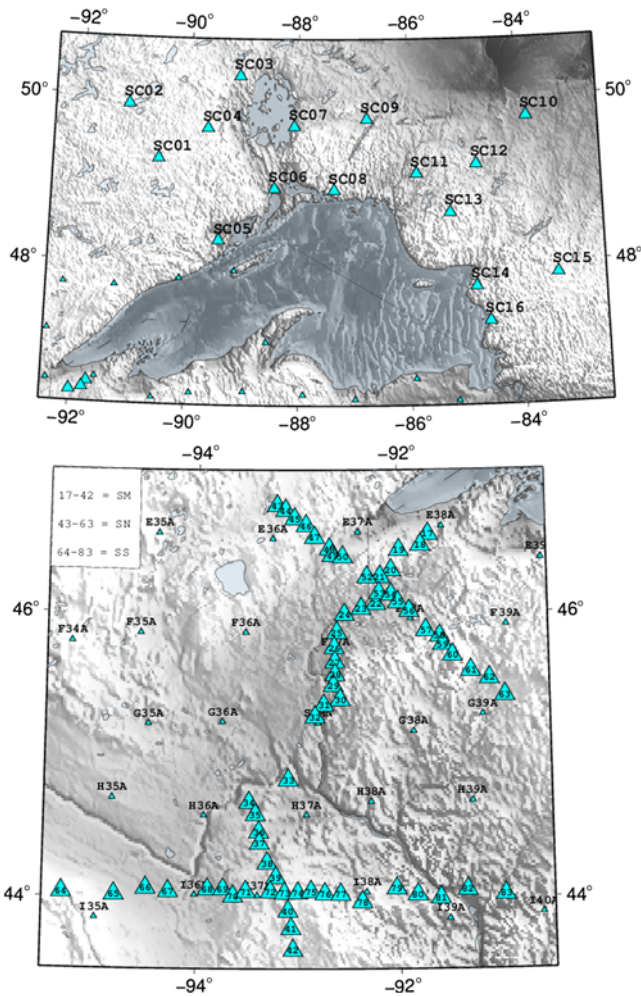


Figure 1. Topographic map of Superior Province Rifting Earthscope Experiment (SPREE) and nearby Transportable Array (TA) stations. Stations SC01–SC16 expand TA-style spacing north of Lake Superior. SM17–SM42 follow the center of the Midcontinent Rift’s Bouguer gravity anomaly. The northern line (SN43–SN63) crosses the anomaly at its widest point, and the southern line (SS64–SS83) crosses it at its narrowest point. The color version of this figure is available only in the electronic edition.

We discuss common sources of noise, explain how we attempted to mitigate the effects of this noise with site selection criteria and installation procedures, and identify the phenomena that generate site-specific long-period noise at SPREE stations.

Sources of Noise

Anthropogenic noise dominates the seismic noise spectrum at short periods (0.1–1 s). This noise is often referred to in the literature as “cultural noise” (McNamara and Buland, 2004) and can be identified by diurnal and work-week variations (Given, 1990; Young *et al.*, 1994). To avoid areas with high cultural noise, sites for SPREE stations were selected based on criteria (Table 1) that were modified from those originally developed for EarthScope’s TA (P. Dorr,

Table 1

Superior Province Rifting Earthscope Experiment (SPREE) Siting Criteria

Feature	Preferred Distance	Minimum Distance
Railroads	10 km	5 km
Highways (interstate)	5 km	3 km
Highways (county)	1.5 km	1 km
Local roads	1 km	500 m
Driveways	400 m	200 m
Occupied buildings	400 m	200 m
Tall objects (trees, towers)	2 × height	1 × height
Oil wells and pipelines	2 km	1 km
Dams	3 km	1 km
Construction	3 km	1 km

personal comm., 2014). Much of the infrastructure in the SPREE area consists of railroads and highways connecting small towns, so avoiding sources of cultural noise proved a challenging task. We generally maintained the suggested minimum 5 km distance from railroads and 3 km from major highways, but it was necessary to place some stations within 200 m of houses or small local roads.

Wind also generates short-period noise. Energy coupled directly into the ground as wind interacts with topography, trees, and buildings is especially troublesome for surface or very shallow installations (Young *et al.*, 1994; Withers *et al.*, 1996).

At periods between 1 and 20 s, the noise spectrum is dominated by oceanic microseisms. Microseisms arise from the conversion of ocean-wave energy into seismic energy, with two peaks between 10–16 and 4–8 s (Longuet-Higgins, 1950; McNamara and Buland, 2004; Ebeling, 2012). This microseismic energy propagates efficiently through the North American crust and is coherently observed throughout the SPREE network, which is over 1000 km from the Atlantic Ocean and at least twice as far from the Pacific and Arctic Oceans. Thus, the power observed in these bands should increase during the northern hemisphere’s winter storm season.

At periods from 20 s to several hundred seconds, local atmospheric and thermal effects, as well as a sensor’s self-noise, tend to dominate the background noise spectrum. Variations in temperature and pressure can create nonseismic noise (i.e., noise not related to elastic deformation of the Earth) by changing an instrument’s response characteristics, by deforming the vault and/or pier or the sensor casing, or by altering the mechanical properties of the man-made or Earth materials surrounding the sensor (Wielandt and Streckeisen, 1982; Holcomb and Hutt, 1992; Bormann, 2009). Therefore, broadband station installation techniques take special care to insulate the sensor from changes in temperature, to minimize airflow and air pressure changes in the vault, and to keep the sensor and the material it sits on from warping or deforming (e.g., guidelines given in Holcomb and Hutt, 1992; Hanka, 2009; Hutt and Ringler, 2009). Regardless of installation, any sensor will generate some amount of self-noise; many

Table 2
Names for Frequency Bands Referred to in the Text

Name	Period (s)	Frequency (Hz)
Short-period or cultural frequencies	0.1–1	1–10
Intermediate-period or microseismic frequencies	1–20	0.05–1
Long-period frequencies	20–800	0.00125–0.05

commonly used broadband sensors exceed the Peterson new low-noise model at periods longer than 100 s (Ringler and Hutt, 2010). Self-noise should be of the same order of magnitude on the vertical and horizontal components.

Atmospheric pressure can also produce “seismic” noise (elastic deformation in the form of tilts and displacements) of the Earth’s surface (Sorrells, 1971; Given, 1990; Bormann, 2009). Tilting produces large apparent horizontal displacements, up to two orders of magnitude larger than those observed on the vertical component (Sorrells, 1971; De Angelis and Bodin, 2012). Unconsolidated sediments are particularly sensitive to variations in atmospheric pressure (Sorrells, 1971). The signal-to-noise ratio of seismic signals can be enhanced at long periods (generally above 100–300 s) by finding the transfer function between atmospheric pressure and seismic noise and removing the atmospheric signal (e.g., Beauquin *et al.*, 1996; Zürn *et al.*, 2007). Unfortunately, fluctuations in atmospheric pressure with periods of hundreds of seconds are only coherent over distances of a few kilometers (Herron *et al.*, 1969; Wilson *et al.*, 2002), so a barometer must be collocated with the seismic station if this correction is to be performed.

Table 2 lists the names used in this text for various frequency bands.

Installation Details

The surface geology in the SPREE study region is dominated by thick layers of soft sediment. With bedrock well out of digging range (except at a handful of sites north of Lake Superior), all SPREE stations were installed in soft sediments. Soils ranged from fertile, farmable loam to sandy glacial outwash plains to clay- and cobble-rich moraine deposits.

Stations were installed using an EarthScope Flexible-Array-Style vault, comprising a 1 m long \times 0.45 m diameter corrugated plastic drainage tube sealed at the base with a rubber membrane and at the top with a specially made watertight cover. We poured approximately 20 kg of grout into the base of each vault, resulting in a pad 15–20 cm thick, and allowed it to cure for at least 1–2 days before installation. Once onsite, we dug a hole slightly larger than the outer diameter of the vault, poured 20 kg of concrete into the hole, inserted the vault, and leveled the vault floor using a spirit level placed on the grout pad. After the concrete had cured for about 30 min, we backfilled soil around the vault and placed the sensor in the vault. All stations initially used Güralp CMG-3T sensors and

recorded datastreams at 1 and 40 samples/s. Two sensors were swapped for Nanometrics Trillium 120 sensors due to sensor failure (SS72 in April 2013 and SS77 in October 2012). To provide additional thermal mass and minimize convection within the vault, we poured clean sand into each vault and tamped it down around the sensor. The vault was sealed with a watertight lid with a ring of plumbers’ putty around the edge. A tarp was placed over the vault and covered with a mound of soil and rocks to provide thermal insulation and deflect water away from the vault.

The REF TEK 130 data acquisition system (DAS), solar panel charge controller, and two 12 V batteries were buried in a large plastic container about 1 m away from the vault. This was also covered with a tarp and a thin layer of soil and/or rocks to hold down the tarp and deflect water. The DAS periodically sent mass-recentering commands to the sensor. Initially, the masses were recentered every 10 days. However, this interval was shortened to 5 days in October 2012 because the mass positions frequently drifted far out of center, especially in the spring. Our analysis now shows that this was due to the stations’ installation in soft soil.

To minimize any confounding effects from slight differences in site construction and sensor performance, this study will focus on a subset of 21 SPREE stations (SM17–SM25 and SN52–SN63) that were installed by the same field team and operated with the same CMG-3T sensors for the entire duration of the experiment.

Data and Methods

To characterize seismic background noise in the SPREE region, we calculate hourly and daily power spectral density (PSD) estimates using the method described in McNamara and Buland (2004). This approach averages 13 75%-overlapping 15-min-long segments per hour to obtain an hourly PSD estimate. These hourly estimates overlap by 50%; all 47 hourly power spectra for a single day are averaged together to obtain a daily power spectrum. Instead of applying the McNamara and Buland (2004) full-octave averaging method to the power spectra, we apply a simple five-point smoothing to the hourly spectral estimates and then interpolate the smoothed curve at evenly log-spaced points. This preserves finer detail within the power spectrum, especially at microseismic and longer periods. Power estimates from SPREE will be compared with the high- and low-noise models of Peterson (1993).

High data returns of > 97% at the TA (Woodward *et al.*, 2013) and > 96% for SPREE (Van der Lee *et al.*, 2013) allow us to characterize temporal variations of the background noise throughout each station’s 2–2.5 year lifetime. To illustrate the variation of noise characteristics over time, we plot spectrograms of the daily PSD curves. The PSD spectrograms are dominated by the persistent long-duration noise that we analyze here. Mass centerings, calibrations, and large earthquakes appear as short-duration, large-amplitude events. Comparison with the Peterson high- and low-noise models

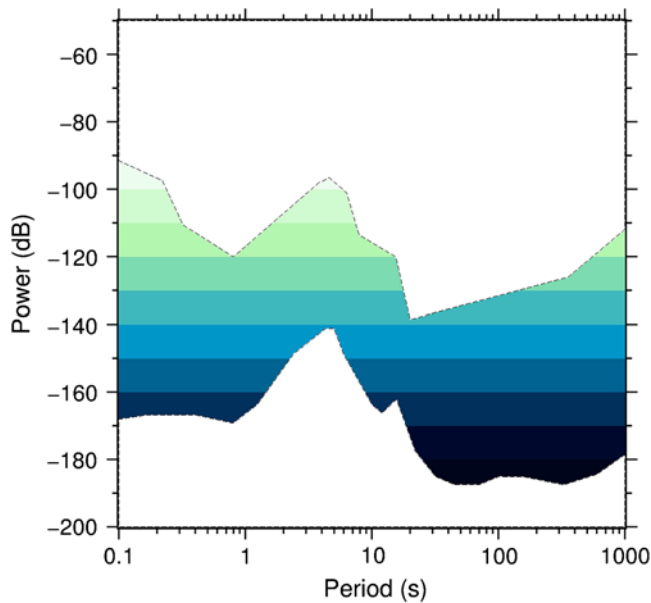


Figure 2. Peterson new high- and low-noise models. Intermediate values are filled using the same scale as Figures 3, 4, and 5. The color version of this figure is available only in the electronic edition.

is facilitated with the legend shown in Figure 2.  Figure S1 (available in the electronic supplement to this article) shows examples of typical SPREE PSD curves produced by earthquakes, quiet and noisy days, and calibration or mass-centering signals.  Figures S2–S7 in the electronic supplement also show difference spectrograms, which were produced by subtracting one PSD spectrogram from another.

We also obtained air and ground temperature data for each station. Air temperature and precipitation data (including snow depth) from weather stations within 10–20 km of each seismic station were obtained from the National Oceanic and Atmospheric Administration (NOAA) National Climatic Data Center (Menne *et al.*, 2012; see [Data and Resources](#)). SPREE stations’ REF TEK 130 dataloggers provided an hourly temperature log in increments of 1°C. Because the DAS was placed in a partially buried box, the DAS temperature acts as a low-passed version of the air temperature. However, because the DAS is only partially buried and surrounded mostly by air, its temperature likely fluctuates more than the temperature of the soil- and sand-surrounded, fully buried sensor. The TA stations’ Quanterra Q330 dataloggers also provide a temperature log, available as channel code VKI (sampled at 0.1 Hz). We decimated these records to 1 sample/hr to match the sampling rate of the SPREE stations. At TA stations, the dataloggers are located in the sensor vault but sit approximately 1–2 m above the sensor and are separated from the sensor by foam insulation (see [Data and Resources](#)).

Because atmospheric pressure variations can produce seismic and nonseismic long-period noise, especially in surface installations, we also computed power spectra for the barometric pressure recorded by the Setra 278 microbarome-

ters at TA stations. These data are available from the Incorporated Research Institutions for Seismology Data Management Center as channel code LDO (for data sampled at 1 Hz). We applied the same method of [McNamara and Buland \(2004\)](#) used for the seismic data. The Setra 278 microbarometer has a simple response given by $P = 800 + 1.5 \times 10^{-4}C$, in which P is the pressure in millibars and C is the instrument output signal in counts. We applied this response correction and converted to units of pascals (Pa) before calculating the power spectral estimates.

Finally, because of the diversity of the surface materials in the SPREE region, we investigated whether noise characteristics correlated with the soil type surrounding a station. Field teams recorded qualitative soil descriptions at stations SC01-16, SM17-25, and SN52-63 when they were removed in October 2013. For stations in the United States, these point observations were compared with the descriptions of soil units provided by the U.S. Department of Agriculture’s Web Soil Survey (WSS; see [Data and Resources](#)). Field observations generally agreed with the WSS, except at a few sites immediately next to farm fields. In those cases, we classify the station according to the observations made at the site. Table 3 lists the field observations and WSS unit and description at each site.

Results

Seasonal Variations

Microseismic noise varies seasonally; as expected, noise between 1 and 20 s increases in power by 10–20 dB during the northern hemisphere winter, when storms are continually generated in the northern Atlantic and Pacific Oceans. This behavior is observed at all SPREE stations; Figures 3 and 4 show examples at stations SM17 and SN52. At periods around 5 s, noise levels are highest during the winter and lowest during the summer. This is typical of stations in the northern hemisphere (Aster *et al.*, 2008). In this period range, vertical and horizontal components show nearly identical noise levels. The central frequency of the secondary noise peak shifts over time due to changes in the strength and position of northern hemisphere storm systems (Sufri *et al.*, 2014). The temporal evolution in strength and frequency content of this noise is similar across the SPREE array (e.g., compare the 5 s curves at the bottom of Figs. 3 and 4), as expected for stations in this region (e.g., [Koper and Burlacu, 2015](#)).

At longer periods, the seasonal trend is the opposite of the trend observed in the microseismic band. At periods greater than 20 s, the horizontal components of many SPREE stations are quietest during the winter, with noise levels up to 20–30 dB lower than in summer. SN52 is one such example (Fig. 3). Between December and March, the average noise level is approximately –150 dB. Between March and May, horizontal noise increases by about 15 dB. Summer and fall noise levels are also approximately 10–15 dB higher than the winter and nearly exceed the new high-noise model

Table 3
Soil Type at SPREE Stations

Station	Field Description	WSS Unit Name and Description
SM17	Sand	Keweenaw, stony–Vilas–Cathro complex: loamy sand
SM18	Loam	Springstead loamy sand, stony: decomposed plant material, loamy sand, gravelly loamy sand
SM19	Fine sand and minor clay	Keweenaw, stony–Newood, stony–Cathro complex: sandy loam, loamy sand
SM20	Sand, clay, cobbles	Newood–Pesabic–Capitola complex, very stony: sandy loam, gravelly sandy loam
SM21	Loamy with minor small cobbles	Milaca–Mora–Haustrup complex, very stony, rocky: silt loam, fine sandy loam, sandy loam, unweathered bedrock at 65–80 in.
SM22	Sand and silt	Grayling sand: sand
SM23	Sand and silt	No data available; possibly Grayling
SM24	Clay and sand with pebbles and cobbles	No data available
SM25	Sand	Meehan sand: sand
SN52	Clay and sand with many roots and other organic matter, well-drained	No data available
SN53	Mostly sand with some clay and silt; well drained	Graycalm–Menagha complex: loamy sand and sand, slightly decomposed plant material
SN54	Sand and a little silt; animal burrows about 2 m to the southeast of vault	Grayling sand: sand
SN55	Sand, with a little silt	Grayling sand: sand
SN56*	Rich, dark brown soil; well-drained mix of clay, sand, silt, organics	Graycalm–Menagha complex: loamy sand and sand, slightly decomposed plant material
SN57	Mostly sand with some pebbles and cobbles	Mahtomedi loamy sand: loamy sand, sand, gravelly coarse sand
SN58*	Soil with organics, clay	Keweenaw–Pence complex, stony: sandy loam, loamy sand, gravelly sandy loam, gravelly coarse sand
SN59	Clay, silt, cobbles; bedrock at ~90 m depth (reported by landowner from well drilling)	Keweenaw, stony–Pence, stony–Greenwood complex: sandy loam, loamy sand, gravelly sandy loam, gravelly coarse sand, peat, mucky peat
SN60	10% organics, 15% boulders, 45% silt, 10% clay, 20% sand	Rosholt sandy loam: sandy loam, gravelly loamy sand
SN61*	Clay with large cobbles; thin surface layer is underlain by Barron quartzite according to landowner (from well drilling).	Santiago silt loam, very stony: silt loam, sandy loam
SN62	60% sand, 30% silt, 10% clay	Scott Lake sandy loam: sandy loam, gravelly loamy sand
SN63	40% sand, 45% silt, 15% clay	Billyboy silt loam: silt loam, loam, sandy loam

WSS, U.S. Department of Agriculture's Web Soil Survey (see [Data and Resources](#)).

*A discrepancy between field observations and WSS classification.

(Peterson, 1993). Noise steadily decreases by 5–10 dB in mid-to-late December. Similar trends in noise power, but with smaller amplitudes and a lower mean, are also observed on the vertical component.

Not all SPREE stations show a pronounced increase in long-period noise during the summer. At SM17, horizontal long-period noise power at 100 s increases by only about 5 dB in the summer, remaining between –150 and –140 dB throughout the year (Fig. 4). Thus, at long periods, the horizontal components of SM17 are slightly quieter than SN52 during the summer and slightly noisier during the winter. This is further illustrated by subtracting the PSD spectrograms of the two stations (Ⓔ Fig. S2). At long periods, the horizontal components of SM17 are quieter than those of SN52 between April and August. The two stations have similar noise levels between September and November, with SM17 beginning to be slightly noisier than SN52. SM17 is consistently noisier than SN52 between December and March.

For TA stations with a very low-noise floor, such as backbone station SPMN, noise at periods longer than 30 s is

lowest during the summer and increases by about 10 dB between November and March on all three components (Fig. 5). This is the opposite of the behavior observed at stations like SN52. Throughout the winter, noise at 100 s remains around –175 dB on the vertical component and –145 dB on the horizontals. This approaches or exceeds the noise level of many SPREE stations. Subtracting the PSD spectrograms of SPMN and SM17 or SN52 shows that, for parts of the winter, SN52 and SM17 experience less horizontal noise above 20 s than SPMN (Ⓔ Figs. S3 and S4). These difference spectrograms also highlight the coherency of microseismic noise power across the SPREE region, regardless of installation type.

Time-of-Day Variations

During summer daylight hours, horizontal long-period noise at SPREE stations increases by up to 30 dB. This variation is comparable to or larger than the seasonal variations described in the preceding section. As shown in Figure 6, this day–night difference has a nearly square-wave profile with a 24-hr period during the summer. At SM17, the difference in

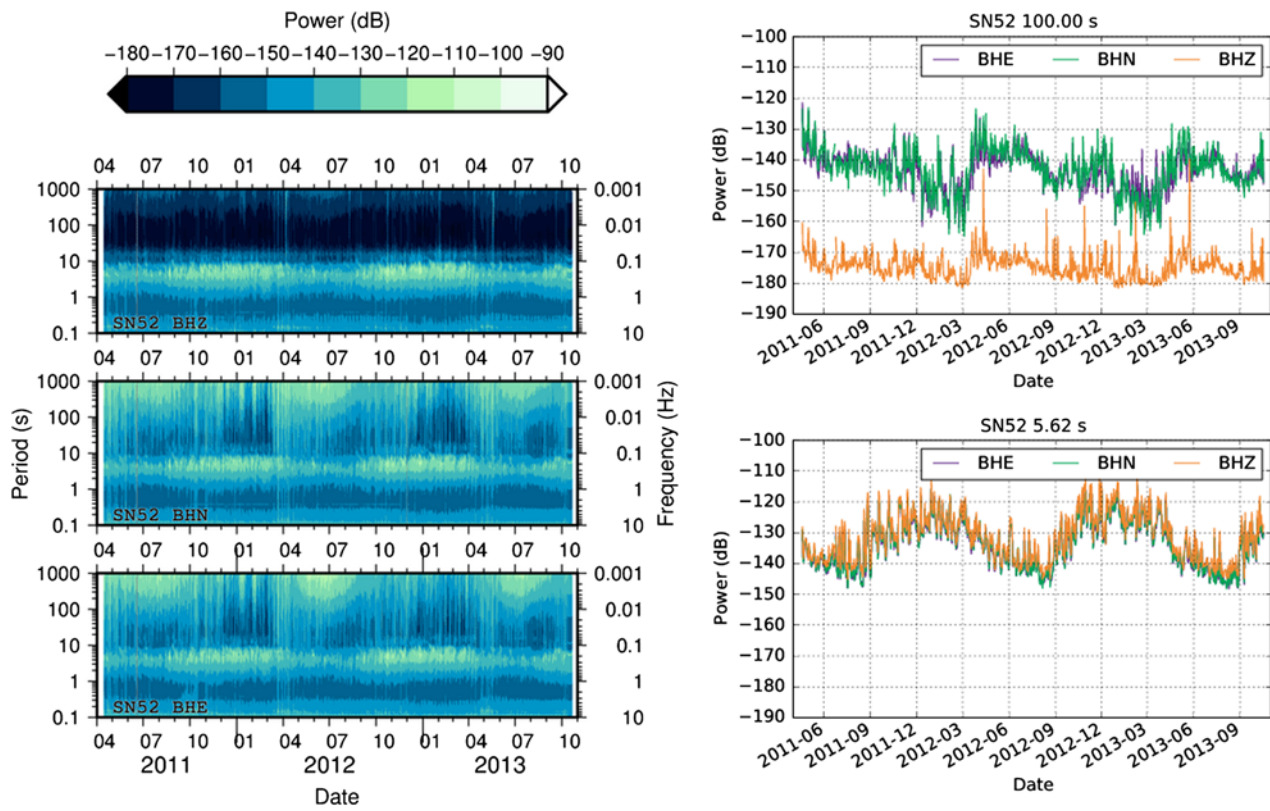


Figure 3. Spectrogram of daily average power spectral densities (PSDs) at station SN52 for 2.5 years, including slices at 5 and 100 s. The color version of this figure is available only in the electronic edition.

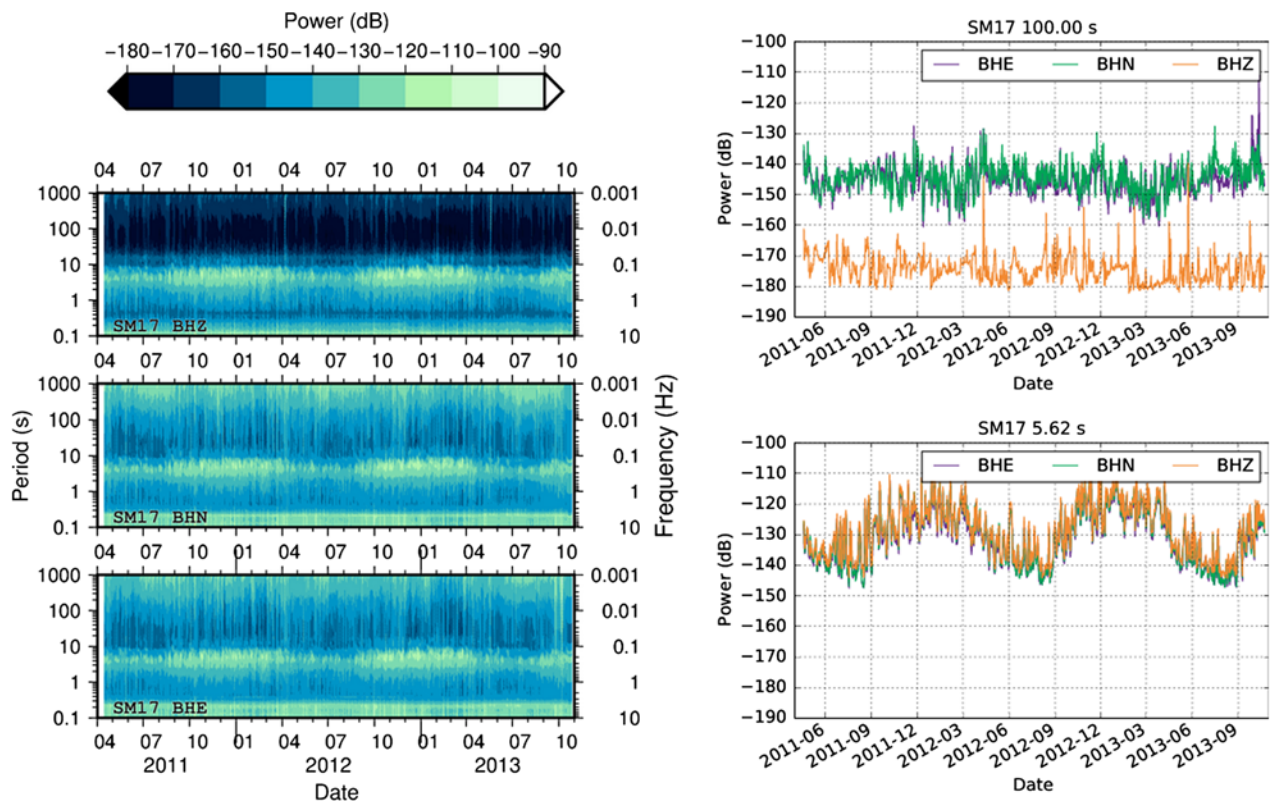


Figure 4. Daily average PSDs at station SM17 for 2.5 years, including slices at 5 and 100 s. A possible horizontal-to-vertical resonance peak is visible between 0.25 and 0.3 s (3–4 Hz). The color version of this figure is available only in the electronic edition.

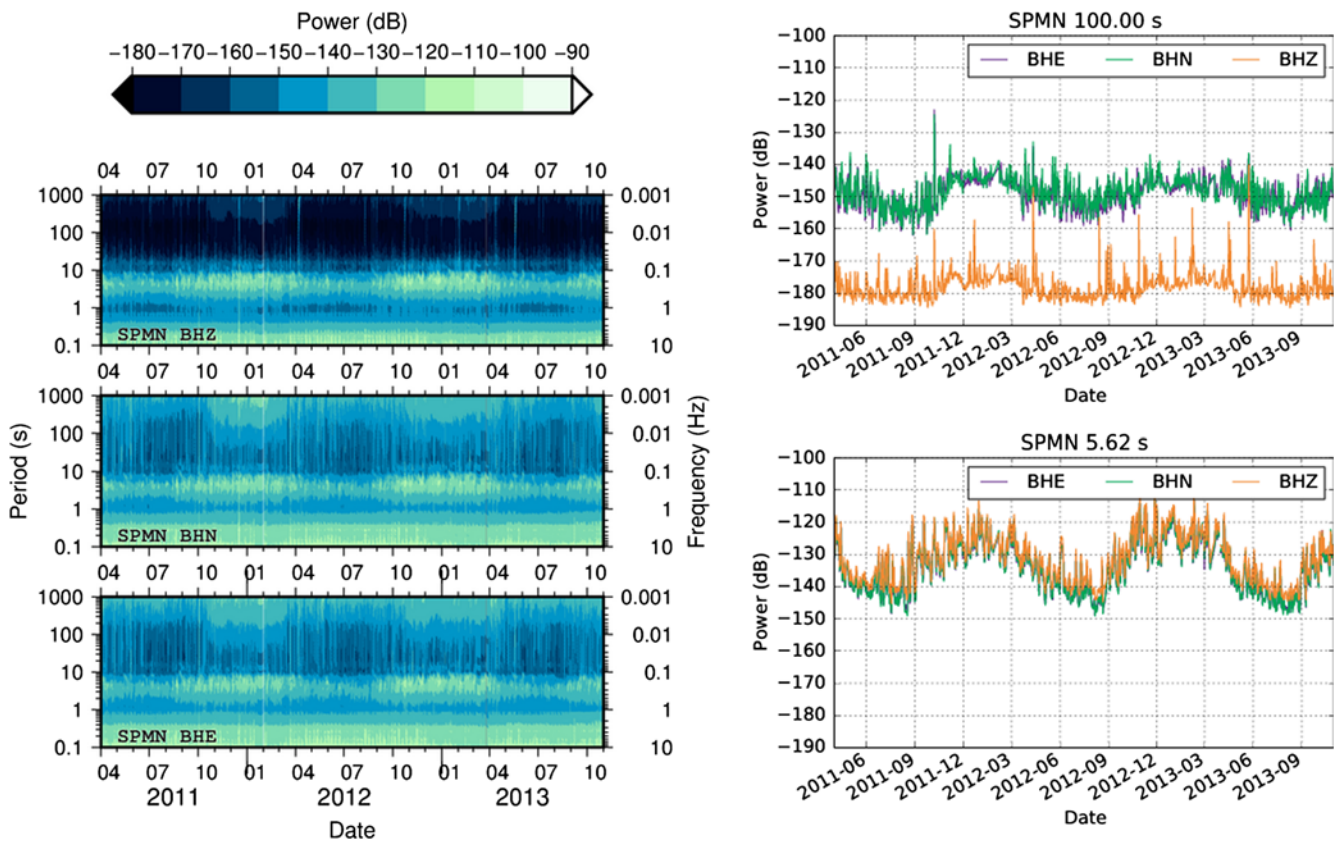


Figure 5. Daily average PSDs at station SPMN for 2.5 years, including slices at 5 and 100 s. Noise between 0.1 and 1 s is higher than in Figures 3 and 4, possibly due to SPMN's proximity to Minneapolis–St. Paul, the St. Croix River, and/or farm buildings on the property. The color version of this figure is available only in the electronic edition.

noise power between summer days and nights often reaches 20 dB. Noise at SPMN also increases during summer days, although the difference between day and night is closer to 10 dB (Fig. 7).

In contrast, this square-wave behavior is absent during the winter (Figs. 6 and 7). At SM17, power still varies considerably from day to day, but its behavior is aperiodic. At SPMN, winter power levels are nearly constant compared to SM17.

A continuous wavelet transform (Kristeková *et al.*, 2009) of the noise power at 100 s from the entire 2.5 year deployment of SM17 (Fig. 8) shows that the noise power varies with a strong 24 hr period on the horizontal components during the summer, with overtones also at 12, 8, and 6 hr periods. This reflects the square-wave profile of the noise seen in Figure 6. The vertical component also has peaks at 24 and 12 hrs, but their spectral amplitudes are 4–6 times weaker than on the horizontal components and do not show the same strong summer–winter difference. Short, strong bright lines on the vertical component are due to large earthquakes. (Visible events include the April 2011 M_w 8.6 Sumatra earthquake, the October 2012 M_w 7.8 Queen Charlotte Islands earthquake, and the May 2013 M_w 8.3 Okhotsk earthquake.)

The LDO (atmospheric pressure) channels of nearby TA stations E38A, F38A, and SPMN also show strong 24- and 12-hr periodic components in summer but not winter at 100 s

(Fig. 9). This difference between summer and winter is less pronounced than for the horizontal components of SM17. In summer, SM17's days are usually 20–30 dB noisier than nights on the horizontals. The diurnal difference in atmospheric pressure during the summer is about 5–10 dB. (The diurnal difference in horizontal seismic noise on the TA stations, not shown here, is typically 10–15 dB; the diurnal difference is negligible on the vertical component.)

Soil Type

SPREE stations installed in fine-grained, organic-rich soil consistently suffer from more horizontal long-period noise than nearby stations in sandy soils or glacial till. For example, SN52 and SM21 are separated by 10 km and are installed in different types of soil. SN52 is in a mixture of clay, sand, and cobbles on a small hill surrounded by low-lying marshy areas, whereas SM21 is in silty loam on a plain about 50 m from a small, slow-moving stream. Horizontal long-period noise levels at SM21 are consistently higher than SN52 by 10–20 dB during the summer (© Fig. S5). During the winter, this difference decreases to a few decibels. The vertical component of SM21 is always quieter than that of SN52.

SN55 and SN56 provide another example of neighboring stations in different soil types. SN55 is in a soil com-

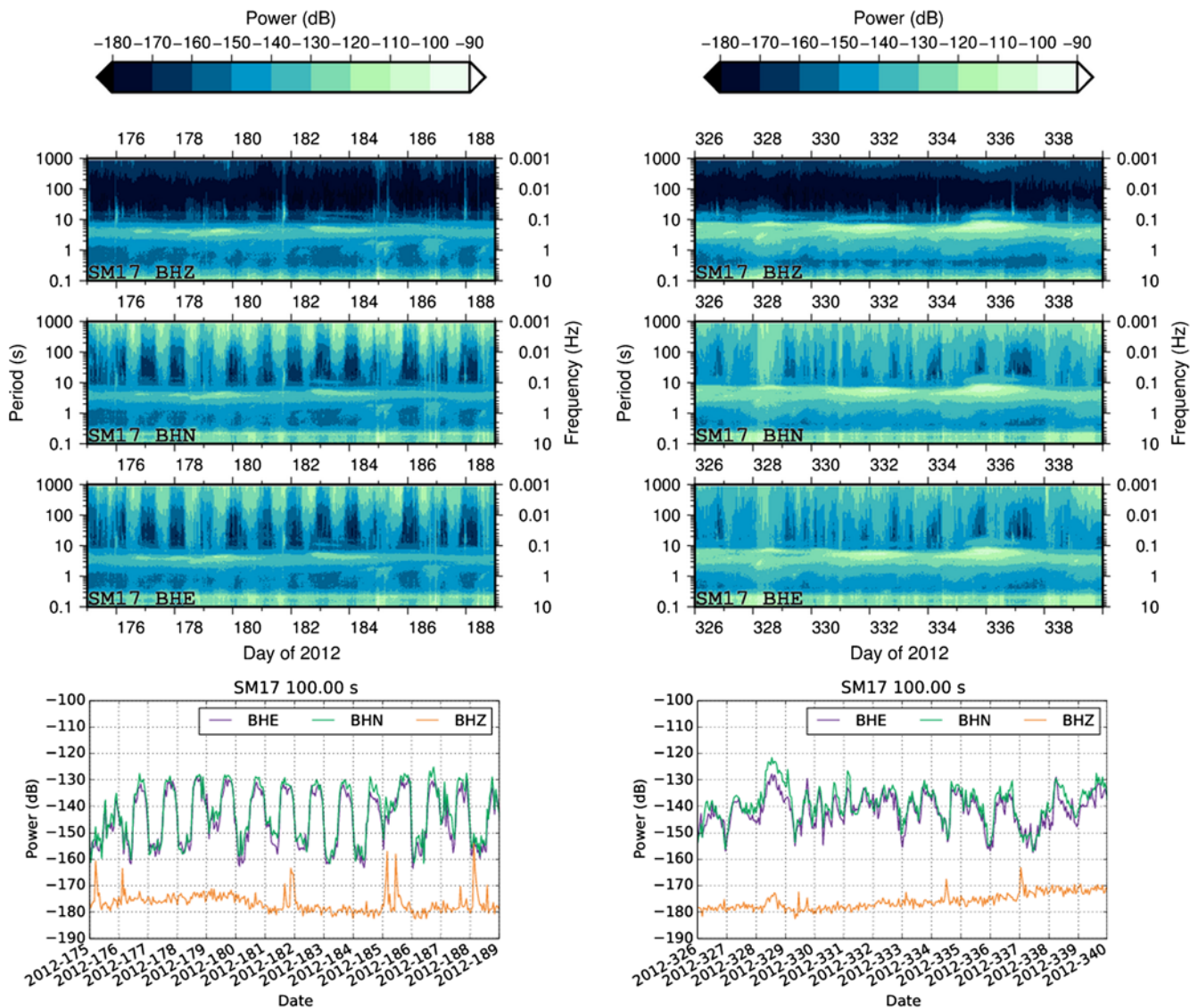


Figure 6. Power at SPREE station SM17 for 14 days in (left) summer and (right) winter, including slices at a period of 100 s. Ticks are at midnight UTC; local time is UTC – 5 during summer and UTC – 6 during winter. The color version of this figure is available only in the electronic edition.

posed of nearly pure sand, called the Grayling soil unit, whereas SN56 is in loamy, organic-rich soil next to a farm field. $\text{\textcircled{E}}$ Figure S6 demonstrates that noise on all components of SN56 increases drastically in the spring and fall. During the winter, however, SN56 is slightly quieter at long periods than SN55.

In contrast to the preceding two pairs of stations, SN54 and SN55 are both installed in the Grayling sand. At periods above 30 s, noise levels at these two stations generally agree within 5 dB ($\text{\textcircled{E}}$ Fig. S7), except for a few periods of excessively high noise of unknown origin at SN54 in May–June 2011 and April 2012.

The lifetime mean PSDs of the five stations discussed previously confirm that the horizontal components of SM21 and SN56 are noisier than their neighbors at periods greater than 30 s ($\text{\textcircled{E}}$ Fig. S8). The lifetime mean PSDs of the

remaining SPREE stations in very silty or very sandy soil show a marked contrast in their horizontal long-period behavior (Fig. 10). All four stations in the Grayling sand unit show remarkably similar horizontal long-period noise levels, and they are some of the quietest stations in the SPREE network. Silty stations, on the other hand, are nearly 10 dB noisier than the Grayling stations. Vertical noise does not appear to correlate with soil type at SPREE stations.

Response to Temperature

An interesting relationship between snow cover, DAS temperature, and long-period horizontal noise power can be seen for stations in fine-grained materials such as SN56 (Fig. 11). During the winter of 2011–2012, snow cover is sporadic for most of the winter and accumulates very gradually. Daytime air temperatures also remain above or very

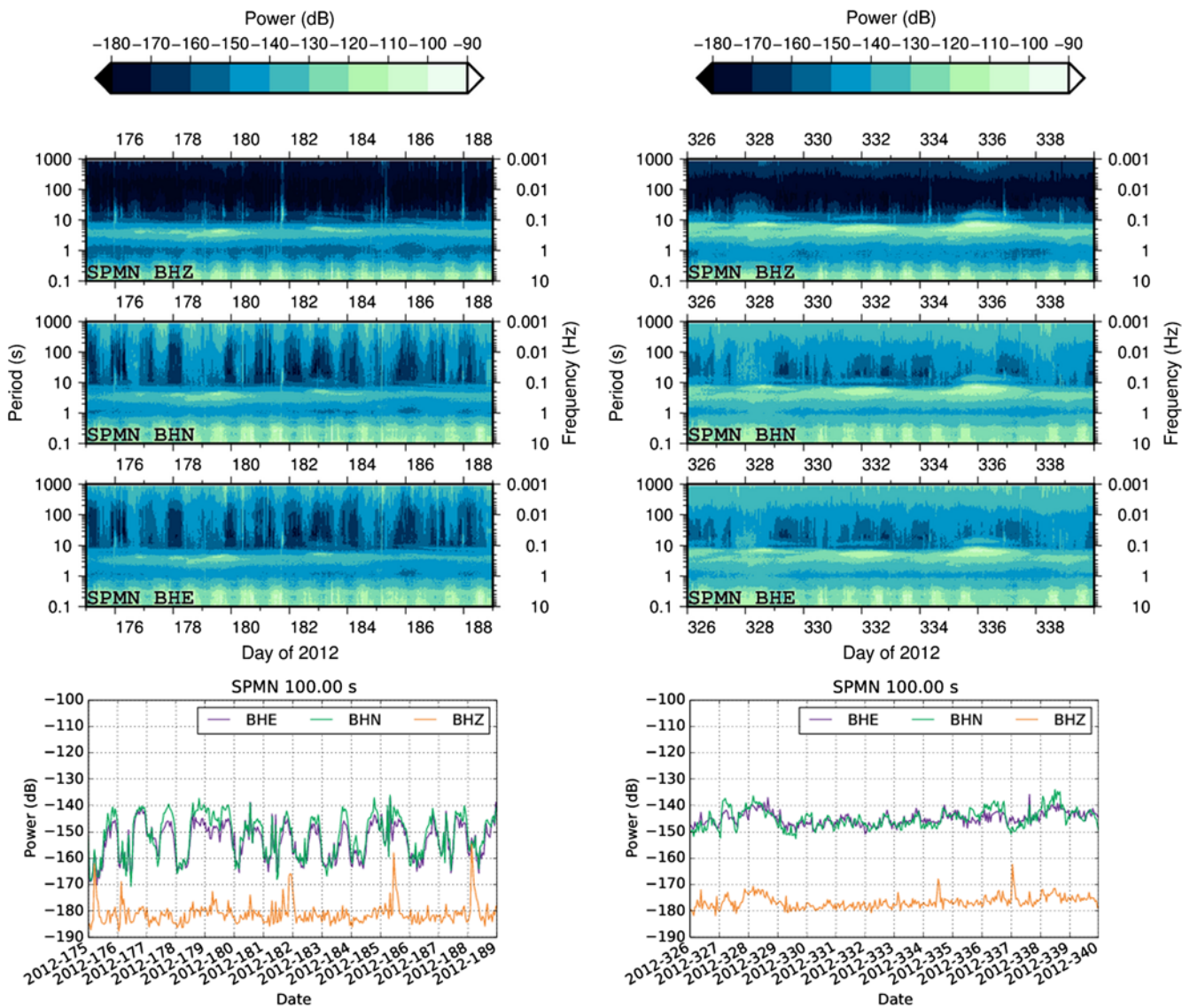


Figure 7. Power at TA station SPMN for 14 days in (left) summer and (right) winter, including slices at a period of 100 s. Ticks are at midnight UTC; local time is UTC – 5 during summer and UTC – 6 during winter. The color version of this figure is available only in the electronic edition.

close to 0°C for much of the winter. As a result of the insulating snow cover and relatively warm daytime temperatures, DAS temperatures do not drop much below –1°C throughout the winter. During this time, the decrease in 100 s horizontal noise at SN56 is also fairly gradual, reaching a minimum during mid-March. Around March 10, snow cover disappears and the DAS and air temperature increase above 0°C. At the same time, horizontal noise increases sharply by 20 dB.

During the winter of 2012–2013, snow cover accumulates rapidly. Maximum daily air temperatures remain below freezing starting in mid-December, coincident with a sharp 15 dB decrease in long-period noise. Long-period noise power remains low for several months and begins to rise in late April when the snow melts and minimum daily air temperatures consistently remain above freezing.

The daily average long-period noise spectrum of the barometric pressure at nearby TA station F38A (Fig. 11, bottom) does not decrease in power during either winter. Daily average noise levels on the horizontal components of F38A and adjacent SPREE station SN55 (in sandy material) also remain relatively constant throughout the year.

Figure 12 further illustrates the differences in behavior between daily mean noise at SN56, SN55, and F38A with respect to daily mean DAS temperature. At SN56, the highest noise occurs at DAS temperatures between 0°C and 10°C, and noise below –150 dB is seen only for temperatures less than 0°C. (This behavior is similar to the previously described SN52; Fig. 3). In contrast, noise power at SN55 has at best a weakly linear relationship with DAS temperature, most notably on the BHZ component. Noise levels at F38A appear to have no relationship with the temperature in the vault.

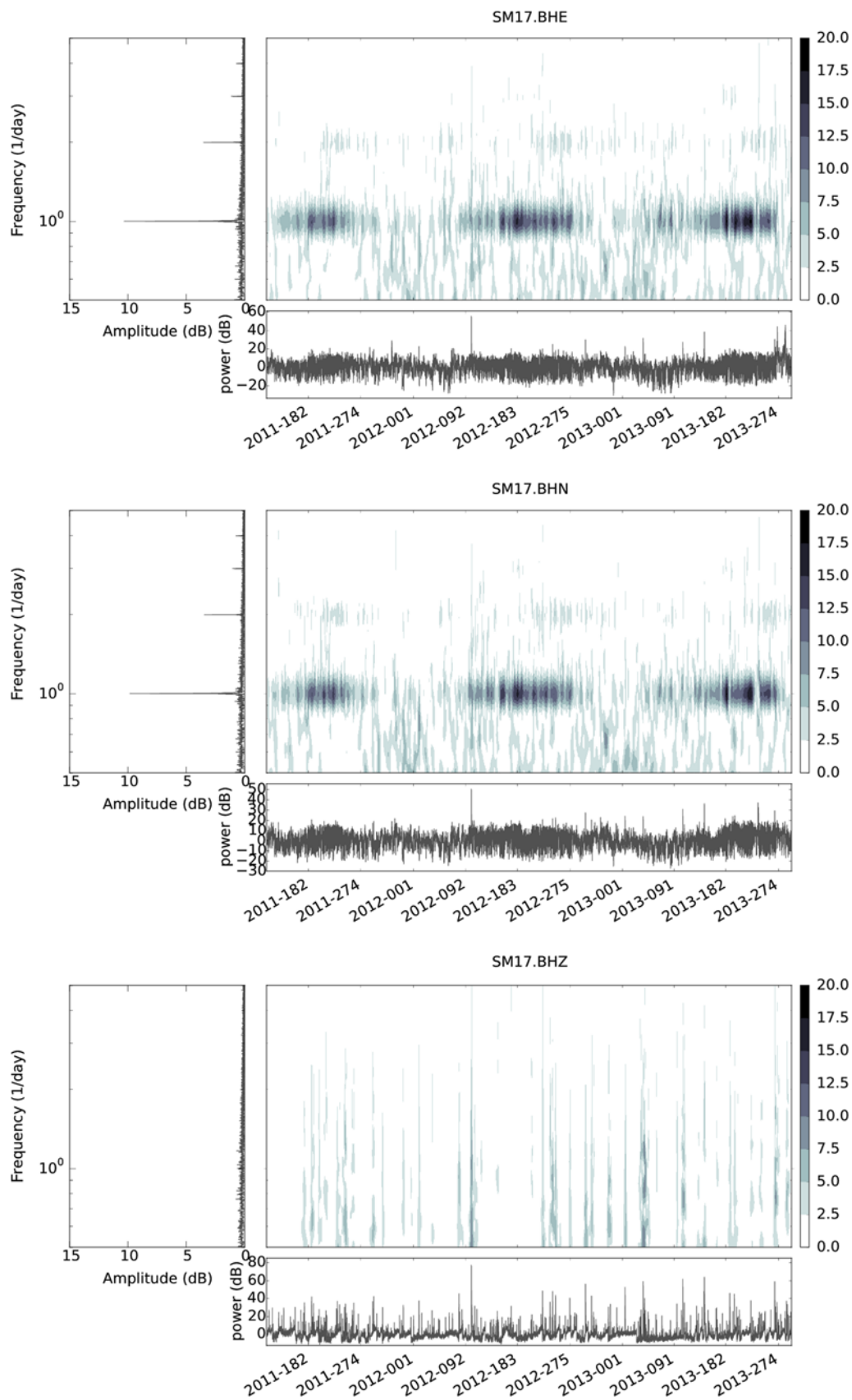


Figure 8. Time–frequency representation of power at 100 s at SPREE station SM17 for 2.5 years. Horizontal components show clear spectral peaks at periods of 24, 12, 8, and 6 hrs (1, 2, 3, and 4 cycles/day). Energy at these periods is strong during summer and decreases during winter. These peaks are absent on the vertical component. The color version of this figure is available only in the electronic edition.

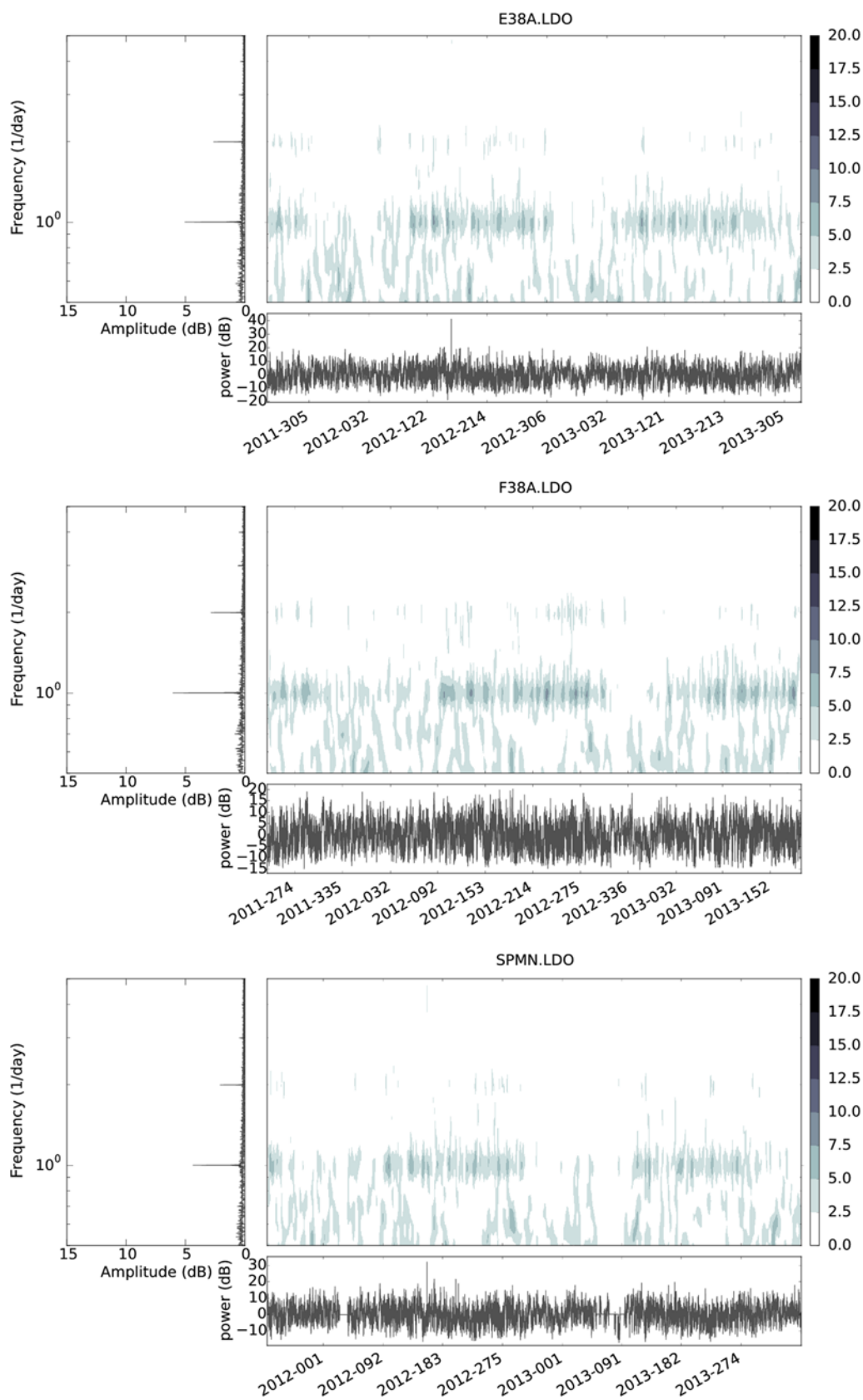


Figure 9. Time–frequency representation of power at 100 s for the barometric pressure recorded at TA stations E38A, F38A, and SPMN during the 2.5-year window in Figure 8. Again, 24- and 12-hr periodic components are present during the summer and absent in the winter. During the summer, power is high during local daylight hours and low in the night. The color version of this figure is available only in the electronic edition.

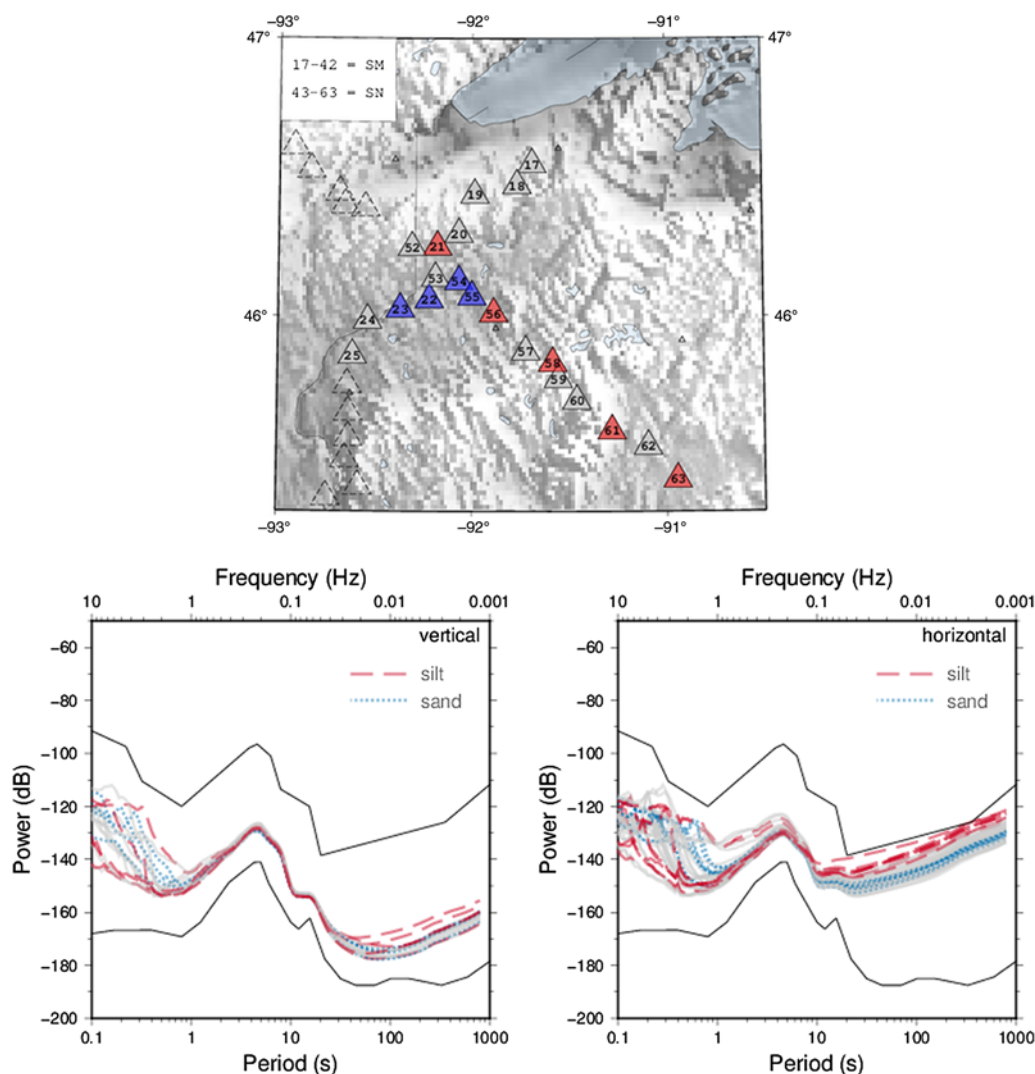


Figure 10. Lifetime average power spectra for SPREE stations SM17-25 and SN52-63. Stations in fine-grained, organic-rich material (SM21, SN56, SN58, SN61, SN63) have higher average horizontal long-period noise levels than their neighbors. In contrast, the four stations in the Grayling sand unit (SM22, SM23, SN54, and SN55) are some of the quietest stations and differ by only a few decibels at long periods on the horizontal components. The color version of this figure is available only in the electronic edition.

Because changes in temperature cause thermal expansion and contraction, we also investigated the relationship between daily mean noise and the daily temperature change (Fig. 13). At SN56 and SN55, the relationship between daily mean noise and daily temperature change is unclear. There may be an increase in noise with daily temperature change, but considerable variation in seismic noise is observed for even small temperature changes of 1°–2°C at both stations. This is especially true of SN56, where noise levels range between –160 to –120 dB for a temperature change of 1°C. The vault temperature of F38A is quite stable, and the small changes in temperature do not seem to affect noise levels.

Response to Pressure

Horizontal noise levels at all three stations have a linear relationship with atmospheric pressure noise, as shown in Figure 14. SN55 and F38A, due to their relatively constant

noise levels, clearly show a linear relationship with atmospheric pressure noise. Winter noise at SN56 has a lower mean than nonwinter noise, but both have an approximately linear relationship with atmospheric pressure noise. Vertical noise levels at SN55 and F38A do not show a strong relationship with atmospheric pressure. Vertical noise at SN56 does appear to correlate with atmospheric pressure but mainly for points in the summer. Upon removing the stations, it was noted that SN56 was slightly out of level, so this could have caused pressure-induced tilts to be recorded on the vertical axis as well as the horizontals.

Because seismic noise power seems to have a linear relationship with pressure noise power, we can calculate the ratio of displacement and pressure spectra to determine the amplitude of the transfer function between them. (We convert to displacement and use units of nm/ μ bar here for later comparison with values from Sorrells, 1971.) Figure 15

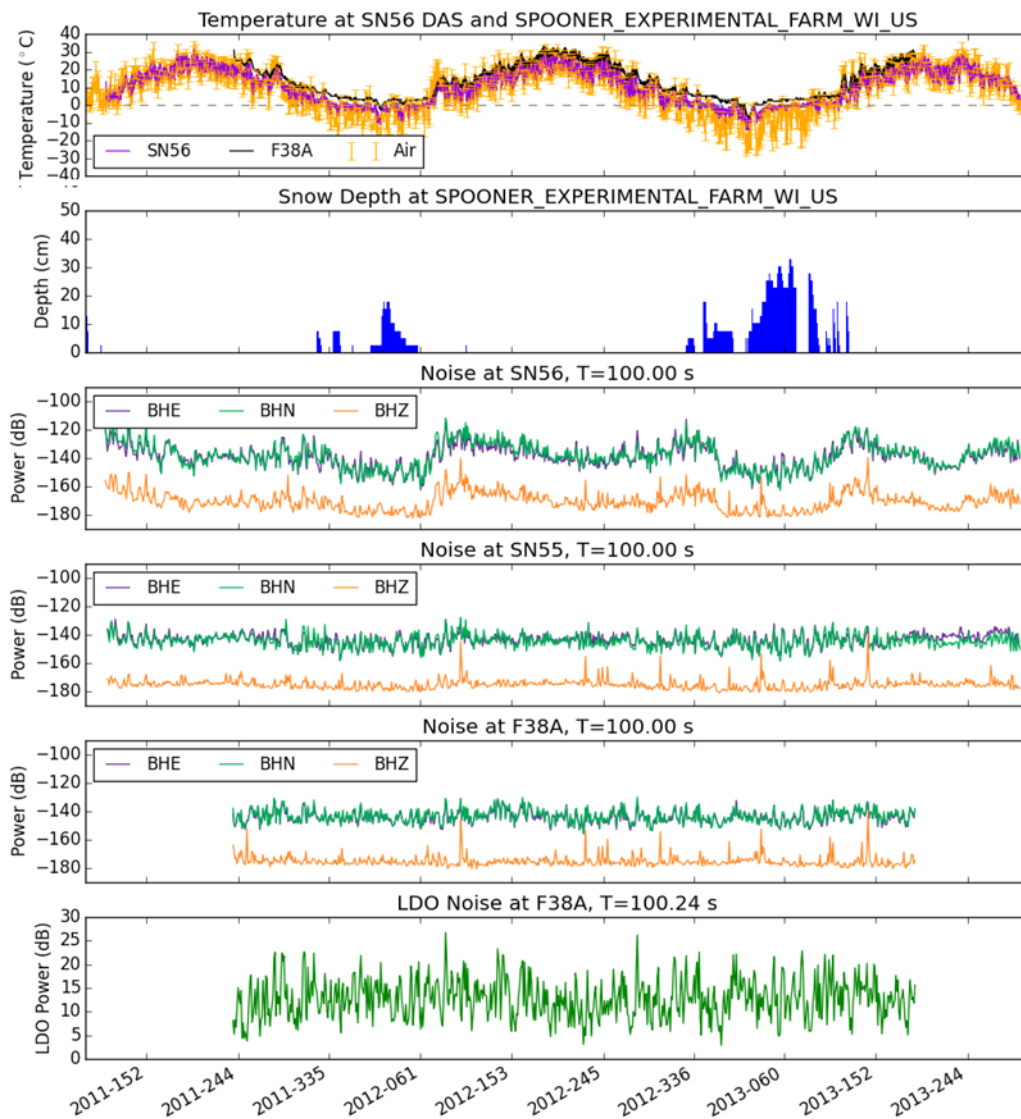


Figure 11. Noise at 100 s decreases at SN56 during the winter, while the ground is frozen and covered with snow. Compared with SN56, horizontal long-period noise at SN55 does not change much throughout the year. Minimum and maximum daily air temperatures from a nearby GHCN climate station (Menne *et al.*, 2012) and hourly temperatures recorded by the DAS at SN56 and F38A are shown. (DAS temperature at SN55, not shown, is within 1°–2°C of SN56.) The daily mean power at 100 s on BHZ, BHN, and BHE channels is plotted for SN56 and nearby TA station F38A. Daily mean power at 100 s is also shown for the atmospheric pressure at F38A. The color version of this figure is available only in the electronic edition.

shows that the ratio of displacement to pressure varies considerably with time at SN56, ranging from approximately 1×10^4 nm/ μ bar during winter to nearly 1×10^5 nm/ μ bar during spring and fall. At SN55 and F38A, the ratio remains roughly constant at just under 2×10^4 nm/ μ bar, increasing slightly during the summer.

Discussion

Long-Period Noise Not a Result of Convection in Vault

We first observed a daytime increase in long-period noise during the first SPREE service run in June 2011. Initially, we attributed this to air convection within the vault

or uneven heating of the sensor; during installation, we added only enough sand to the vault to barely cover the sensor. This left a gap of several tens of centimeters between the sand surface and the vault's lid. In October 2011, we added more sand to the vaults, covering the entire sensor and reducing the gap between sand and lid to about 20 cm. Despite these efforts, we did not observe a reduction in long-period noise, indicating that the observed seasonal and diurnal noise variations are generated by some factor other than air convection within the vault.

Seasonal Noise Variations

We resolve an increase in power at SPMN at periods > 100 s during the winter months (Fig. 5). The timing and

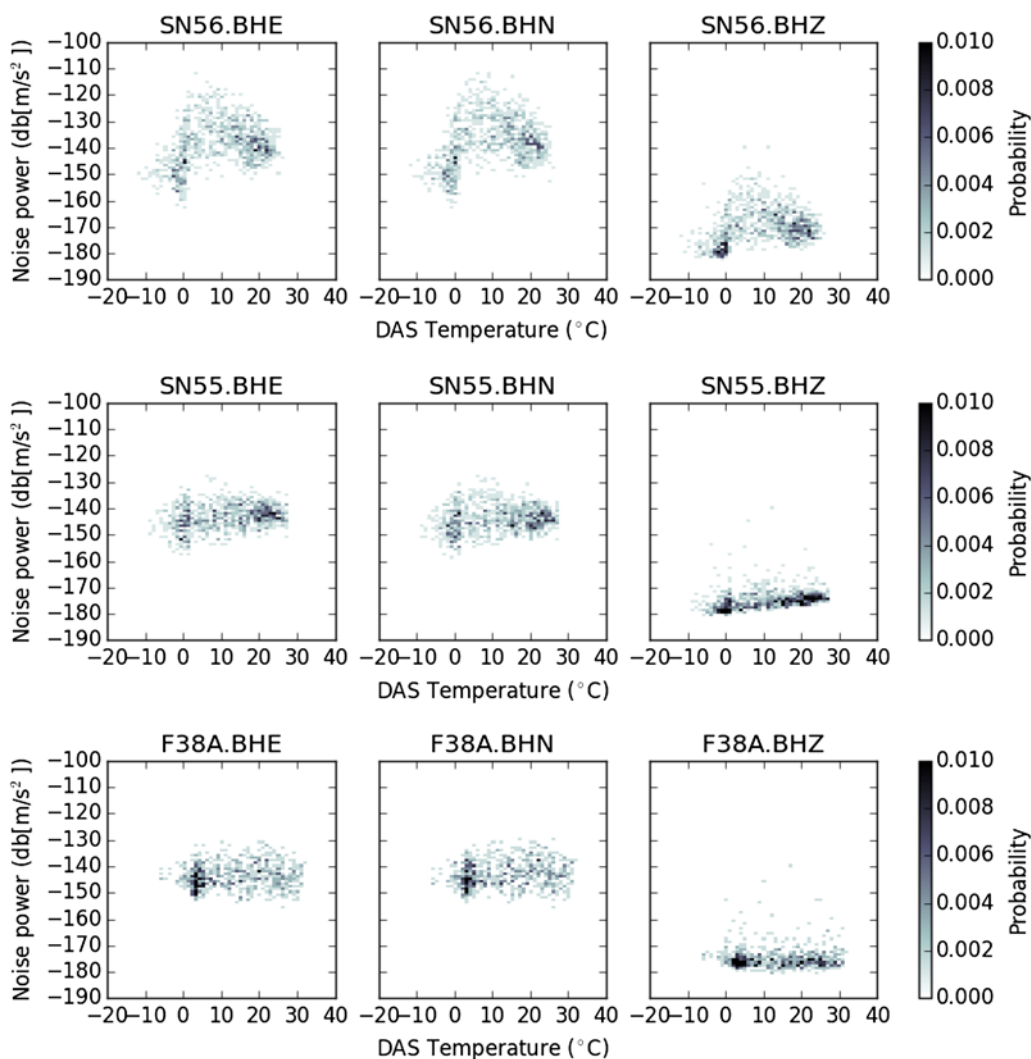


Figure 12. Daily mean noise versus daily mean temperature at SN56, SN55, and F38A. SN56 is noisiest at temperatures between 0°C and 10°C and quietest below 0°C. Noise at SN55 increases slightly with temperature; this is clearest on the vertical component. Noise at F38A does not vary with temperature. The color version of this figure is available only in the electronic edition.

frequency content of this noise, together with the fact that it coincides with a 10–20 dB increase in microseismic noise, suggests that it is the long-period hum created by winter storms and/or the waves they generate (Rhie and Romanowicz, 2004; Webb, 2007; Nishida, 2013).

Previous studies observed an increase in permanent stations’ horizontal long-period noise during the winter, similar to the behavior of SPMN and other TA stations. A 10–12 dB increase in noise between 10 and 100 s during the winter at the Norwegian Seismic Array (NORSAR; Ringdal and Bungum, 1977) was attributed to storms in the Atlantic Ocean. Vila (1998) and Vila and Macià (2002) found that noise at station CADI increased during winter and decreased during summer for periods between 1 and 100 s. They also noted that the double-frequency microseismic peak tended to shift toward longer periods during the winter, a phenomenon that is clearly recorded in the PSD spectrograms of all TA and SPREE stations.

In contrast to TA stations, SPREE stations tend to be quietest in the winter while the ground is frozen. During this time, their long-period noise power approaches that of nearby TA stations. In the spring, summer, and fall, noise levels increase up to 20–30 dB at some stations. This will be further explored in the [Soil Characteristics Determine Response to Pressure and Temperature](#) section.

Origin of 24 Hr Noise Modulation

During the summer, we observe a 24 hr modulation in the power spectrograms of both atmospheric pressure and seismic noise at periods between 20 and 800 s. The existence of a 24 hr variation in surface pressure and surface wind speeds is well known (Dai and Deser, 1999). These, along with other variations at integral fractions of a 24 hr day, are driven by atmospheric tides (Chapman and Lindzen, 1970; Dai and Deser, 1999; Dai and Wang, 1999; Ray and Ponte, 2003). At the latitude of SPREE stations, the diurnal

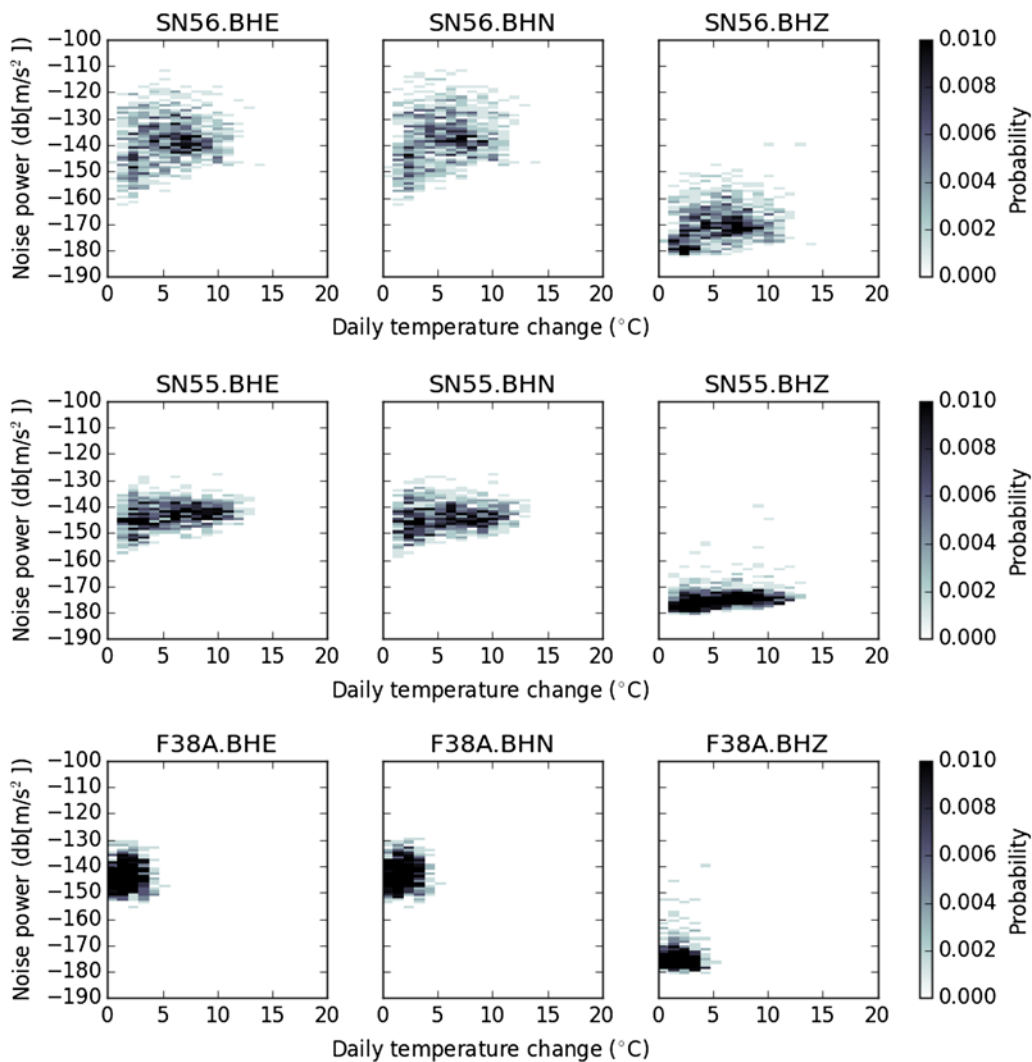


Figure 13. Daily mean noise versus daily temperature change at SN56, SN55, and F38A. Noise at SN56 appears to depend somewhat on the daily temperature change. At SN55, temperature changes appear to have a smaller effect on noise levels. At F38A, the vault temperature is more stable than at the SPREE stations and appears to have little effect on noise levels. The color version of this figure is available only in the electronic edition.

tide variation S_1 reaches maximum daily amplitude between 1500 and 1700 UTC (10 a.m. and noon locally) (Dai and Wang, 1999). S_1 has a strong nonmigrating component that is strongly influenced by sensible heating from the ground surface (Tsuda and Kato, 1989; Dai and Wang, 1999). It is therefore strongest over large land masses such as North America, and it reaches its maximum in summer (Dai and Wang, 1999). Speeds of surface winds, which are driven by variations in atmospheric pressure, also reach their maximum daily speed around early afternoon (Dai and Deser, 1999).

These characteristics accord with observations of atmospheric pressure and seismic noise (Figs. 6–9). A similar modulation of seismic noise was linked to atmospheric tides by Custódio *et al.* (2014). They observed a 12 hr variation in 100 s noise that could be related to the semidiurnal S_1 tide, which dominates surface pressure variations in coastal settings (Ray and Ponte, 2003). In the SPREE region, the diurnal varia-

tion in 20–800 s atmospheric pressure amplitudes (which drives the diurnal variation in wind speeds) produces a diurnal variation in horizontal seismic noise levels. This may be due to local tilting of the ground as described in Sorrells (1971), or it may be due to other, nonseismic effects. This distinction will be explored further in the following section.

Soil Characteristics Determine Response to Pressure and Temperature

Previous studies observed a diurnal variation in long-period horizontal noise at many broadband stations, even those installed on bedrock. For example, Ringdal and Bungum (1977) observed a diurnal difference on the horizontal components of NORSAR stations, although it was much smaller in amplitude (1 dB) than for SPREE sites. This is likely due to a combination of a much higher-quality permanent installation and the fact that the instrument had minimal

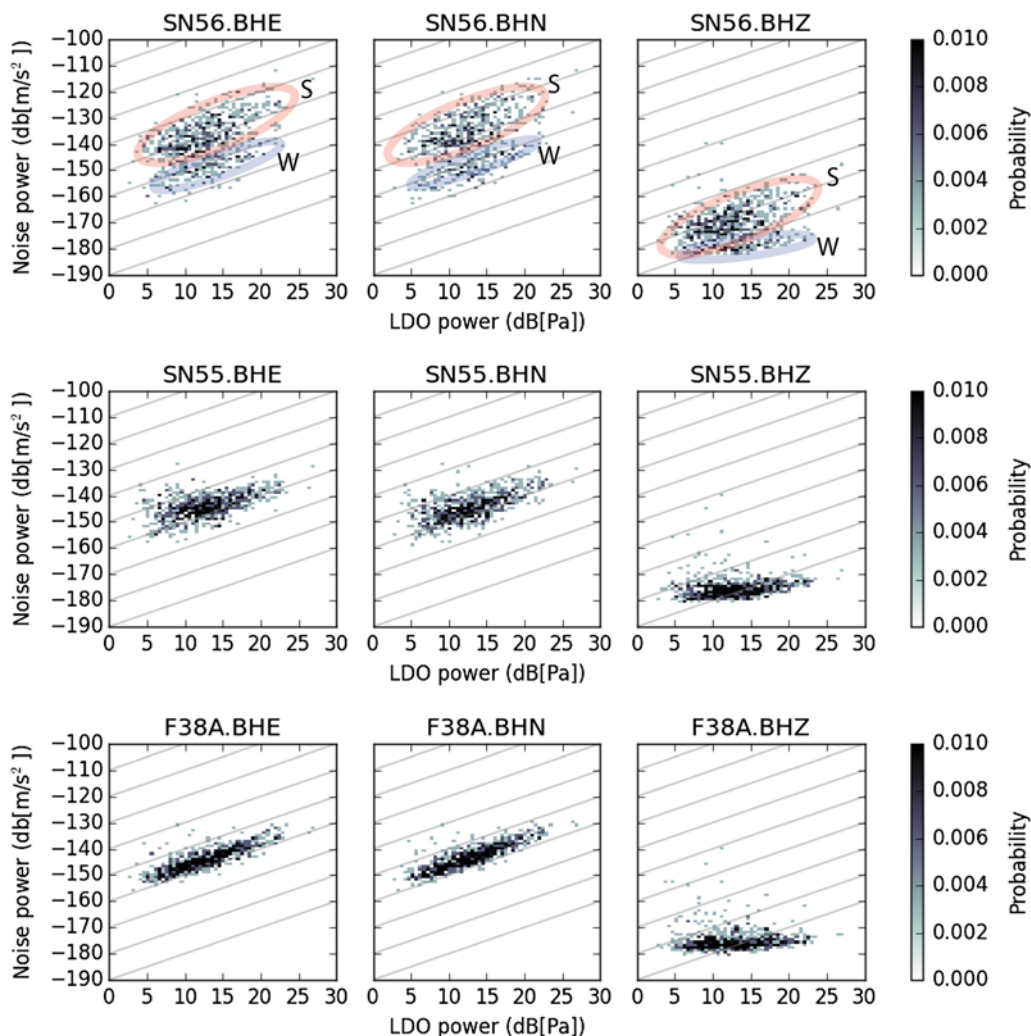


Figure 14. Daily mean noise versus daily mean atmospheric pressure noise (LDO, recorded at F38A). Noise on the horizontal components of SN56, SN55, and F38A all show a linear relationship with atmospheric pressure noise. Diagonal lines indicate a slope of 1. For SN56, the circled areas labeled W indicate values that occur during winter (December–March); values in circled areas labeled S occur during the rest of the year. The color version of this figure is available only in the electronic edition.

sensitivity at periods above 100 s. In a study of noise at GEOSCOPE stations, [Stutzmann *et al.* \(2000\)](#) demonstrated a 10–15 dB daytime increase in long-period horizontal noise at station TAM and many other GEOSCOPE stations. At temporary RISTRA stations in the southwestern United States, a > 7 dB difference between day and night was attributed to some combination of soil conditions, vault geometry, temperature, and/or atmospheric effects, although no systematic assessment of soil type, local temperature, or weather conditions was conducted ([Wilson *et al.*, 2002](#)). They concluded that better characterizing the interactions of thermal and atmospheric pressure effects with vault design and surface geology would constitute a crucial step forward in improving long-period noise characteristics at shallow portable broadband deployments.

We conducted a systematic study of soil conditions, temperature, and atmospheric pressure. One of our major findings is that stations in different types of soil have differ-

ent noise characteristics throughout the year. Stations in fine-grained, organic-rich material, such as SM21, display a 20–30 dB difference between summer day and night noise levels on the horizontal components and a high mean noise level. Daily average power at stations in fine-grained material can be 20–30 dB higher in summer than in winter. Stations in sandy soil, such as SN54, still suffer from a 20 dB increase in long-period noise during summer days, but their mean noise level is typically 10 dB less than stations in silty materials. Sandy stations’ daily average power levels show little difference between winter and summer.

To explain the differences in noise behavior between coarse- and fine-grained materials, we propose that the noisiness of a soil is related to its water content and grain size. Soils of different grain size and moisture content have different thermal and mechanical properties, and the properties of a given soil can vary depending on whether the soil is frozen, freezing/thawing, or unfrozen ([Farouki, 1981](#)).

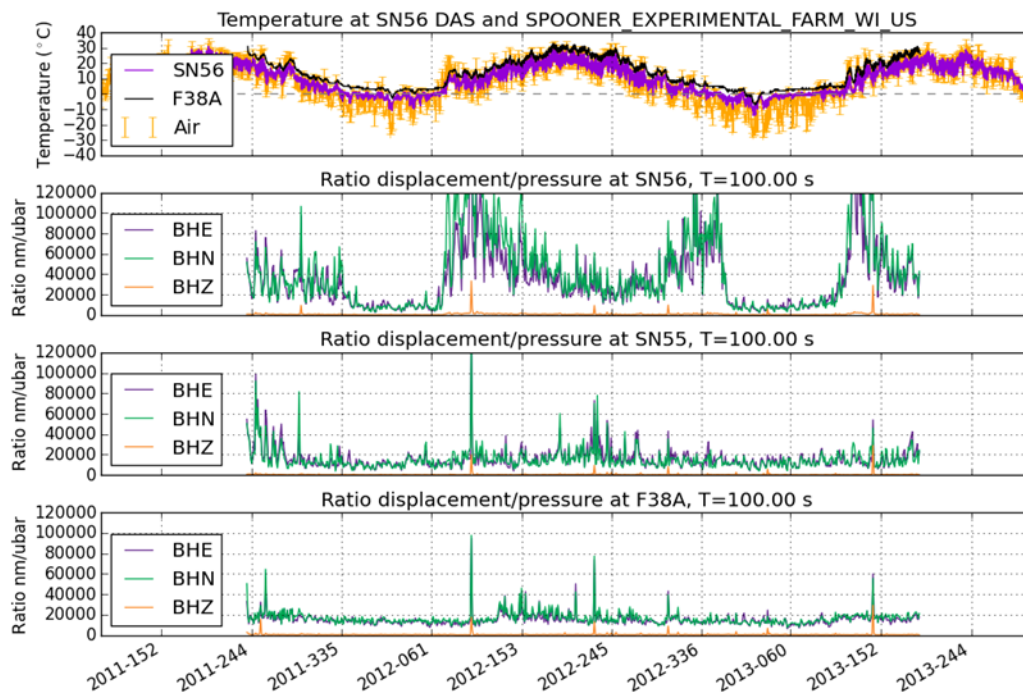


Figure 15. Daily ratio of displacement-to-pressure spectral amplitudes for SN56, SN55, and F38A. (Because SPREE stations did not record atmospheric pressure, the daily displacement spectra of SN56 and SN55 were divided by the daily pressure spectra from F38A.) The displacement-to-pressure ratio at F38A and SN55 remains relatively steady year-round. SN56 shows large displacement-to-pressure ratios in spring and fall that cannot be explained by local ground tilts alone. These large amplitudes coincide with freezing and thawing, as shown by the DAS and air temperatures. The color version of this figure is available only in the electronic edition.

Fine-grained materials and those containing abundant silt, clay, and/or organic material retain more pore water than coarse-grained, sandy materials (Gupta and Larson, 1979). Because water in the soil freezes, it causes a change in volume: silty and clayey materials can increase their volume by more than 10% when freezing, whereas volume changes in sandy soil tend to be minimal (Farouki, 1981). While thawing, meltwater drains quickly from sandy soil but is frequently trapped in the pore space of finer-grained soils (Farouki, 1981). Therefore, we expect large changes in the rigidity and stability of silty and clayey soils while freezing or thawing. Sandy soils should show smaller changes. Given these predictions, we can begin to build a description of the relationships between horizontal noise, soil type, ground temperature, and atmospheric pressure.

Noise levels in fine-grained material seem to be sensitive to the phase of water in the soil: frozen ground is quiet, unfrozen ground is noisier, and ground in the process of freezing or thawing is extremely noisy. That is, temperature has an effect on noise levels because of the water-to-ice phase transition, which is accompanied by a change in mechanical properties. In the SPREE area, the upper 1–1.5 m of ground regularly freezes during the winter (see Minnesota Department of Labor and Industry in the Data and Resources), so the vaults would have been completely encased in frozen ground, especially during the very cold winter of 2012–2013. Other than the solid–liquid phase transition, it seems that the daily temperature (Fig. 12) and daily temperature change (Fig. 13) do

not have a clear correlation with horizontal noise levels. It is well documented that changes in temperature can produce elevated long-period noise at broadband seismic stations (Usher *et al.*, 1978; Wielandt and Streckeisen, 1982); however, for SPREE stations, temperature changes alone cannot explain the observed temporal variations of long-period noise power.

Atmospheric pressure noise does have a strong correlation with horizontal noise at our stations (Fig. 14). Previous work has demonstrated that pressure variations can deform the ground around the sensor, producing a predictable “seismic” signal (e.g., Beauduin *et al.*, 1996; Zürn *et al.*, 2007; De Angelis and Bodin, 2012). However, atmospheric pressure changes can also deform tightly sealed vaults (Holcomb and Hutt, 1992; Beauduin *et al.*, 1996) and alter the height of the water table and the flow of groundwater (Peck, 1960; Spane, 2002). From our data, it is difficult to separate seismic and nonseismic pressure effects. Some insight may be obtained by comparing the observed ratios of displacement to pressure (Fig. 15) with theoretical predictions.

Sorrells (1971) demonstrated that in unconsolidated materials, displacements and tilts due to atmospheric pressure can be quite large. In that study, the worst possible conditions for a surface installation were modeled as unconsolidated sediment with P -wave velocity $\alpha = 0.3$ km/s, S -wave velocity $\beta = 0.1$ km/s, and density $\rho = 1.6$ g/cm³. Unfortunately, these worst-case conditions are typical conditions in the SPREE region (and for many temporary deployments on

continental platforms). [Press \(1966\)](#) notes that soil can have α as low as 0.1–0.2 km/s. Unconsolidated sandy materials and glacial tills, both common throughout the SPREE region, encompass a range of velocities, with $\alpha = 0.2$ –2 km/s.

The predicted apparent horizontal displacement-to-pressure ratio due to tilt for Sorrells' unconsolidated sediment model is approximately 1×10^4 nm/ μ bar at 100 s periods, which agrees well with observations at sandy SPREE stations and TA stations throughout the year and at fine-grained stations in the winter. Fine-grained stations have a slightly higher displacement-to-pressure ratio between 2 – 4×10^4 nm/ μ bar during the summer. These values can also be fit with reasonable values of α , β , and ρ for soils. Indeed, it is expected that velocities in unfrozen ground should be lower than in frozen ground ([McGinnis et al., 1973](#)), which would result in larger displacement-to-pressure ratios in summer. Unfortunately, however, the very large displacement-to-pressure ratios of 8 – 10×10^4 nm/ μ bar calculated for SN56 and other fine-grained stations in the spring and fall cannot be fit by any reasonable values of α , β , and ρ . This is an indication that during the spring and fall, and perhaps in the summer as well, the high noise levels at these stations are probably not produced solely by elastic deformation of the Earth. Instead, a nonseismic source may be involved.

Anomalously high spring and fall noise at SN56 and other fine-grained stations could be caused by changes in the structure and stability of the soil. As noted earlier, freezing and thawing tends to destabilize fine-grained material; it also results in a redistribution of water in the subsurface. Shrinking, expansion, and moisture redistribution tend to occur unevenly during freezing and thawing, especially in clays ([Farouki, 1981](#)). This frost heaving could cause the vault to tilt and shift in the ground. It might also explain why the masses tended to drift out of center rapidly in the spring and fall, requiring extremely short (five-day) recentering intervals to maintain station performance during these times. Discussions with landowners confirmed that frost heaving is a widespread phenomenon throughout the area.

Another possible source of nonseismic long-period noise is warping of the vault due to changes in atmospheric pressure. In studies of noise on high-quality STS-1 installations, [Holcomb and Hutt \(1992\)](#) and [Beauduin et al. \(1996\)](#) observed that horizontal components tended to become noisier when placed under vacuum. This was ascribed to warping of the baseplates on which the sensors rested. Although it is unlikely that SPREE vaults were completely airtight, the tight-fitting lids sealed with plumbers' putty may have partially isolated the vaults from pressure changes. Our concrete piers were coupled to the vaults' walls, so any deformation of the walls due to changes in pressure could result in tilting of the vault floor.

Excess water trapped in freezing or thawing soil may also have exerted pressure on the sides of the vault. Atmospheric pressure variations can cause the height of the water table to vary by up to 10 cm in soils where air is trapped in groundwater, and this effect is largest for soils where the water table is

at or near the surface ([Peck, 1960](#)). During thawing, the boundary between unfrozen ground above and frozen ground below acts as a nearly impermeable barrier to water drainage and traps meltwater within the near-surface soil ([Hayashi et al., 2003](#)), especially in clay and fine-grained soils. Fluctuations in atmospheric pressure can also cause the direction and velocity of lateral groundwater flow to vary ([Spane, 2002](#)). These lateral and vertical changes in the flow of groundwater may have placed additional pressure on the walls of the vault and generated additional nonseismic long-period tilt noise. Sandy soils, which drain quickly, would be less susceptible to these effects than slowly draining fine-grained soils.

In general, sandy soils retain less pore water and experience less structural upheaval during freezing and thawing, which would explain why stations such as SM17 and SN55 show consistent daily mean noise levels throughout the year (Figs. 4 and 11). Fine-grained soils with high moisture contents experience changes in their structure and water content throughout the year. This would explain, for example, why the clayey till at SN52 is consistently noisier than the sand at SM17 during the summer but quiet when frozen in the winter (Ⓔ Fig. S2). Silty SM21 is even noisier than SN52 during the summer but also becomes quiet during the winter (Ⓔ Fig. S5).

Our findings indicate that, for sites where bedrock is far from the surface, it may still be possible to reduce horizontal long-period noise by selecting a site with appropriate soil characteristics. The best-performing SPREE stations were installed in relatively coarse-grained, well-drained, organic-poor soils such as sand or sandy loam. Materials derived from glacial till, consisting of a mix of sand, clay, and cobbles, tended to be noisier than stations in pure sand but performed better than exclusively fine-grained materials or those with abundant organic matter.

Conclusions

Horizontal long-period (> 20 s) noise at SPREE and nearby TA stations varies both seasonally and diurnally. During summer days, SPREE stations are 20–30 dB noisier than during the night. Nearby TA stations are 10–15 dB noisier during summer days than summer nights.

During the winter, noise levels vary considerably from day to day but do not show diurnal periodicity. Some very quiet TA stations, such as SPMN, record an increase in long-period noise during the winter. Because this occurs at the same time that power in the microseismic band increases and shifts toward longer frequencies, it is likely the long-period hum is generated by large storm systems over the oceans.

During the summer, SPREE stations in fine-grained, organic-rich soil show the largest diurnal variation in noise levels. Stations in sandy or better-drained materials are less affected. During the winter, many of the noisiest stations become quiet after the ground freezes and becomes more rigid. Freezing has less of an effect on noise levels at SPREE stations in coarse material and at TA stations. Diurnal variations

in horizontal seismic noise levels diminish in winter for all SPREE and nearby TA stations.

We suggest that atmospheric pressure is the primary source of long-period horizontal noise at SPREE stations and that the effects of pressure variations are modulated by the grain size, frozen or unfrozen state, and moisture content of the surface material surrounding each station. Although the shallow, watertight vault design of SPREE stations produced low vertical noise levels, prevented flooding, and enabled a 96% data return, it may have left the stations vulnerable to frost heaving and to both seismic and nonseismic pressure effects.

We encourage investigators who deploy temporary seismic stations in soft sediments to note the characteristics of the material surrounding their stations. At minimum, this should be a qualitative description of material grain size and organic content that can be checked against a published soil survey. Additional data, such as barometric pressure, vault temperature, soil moisture content, and soil permeability, would aid in characterizing the relationship between long-period noise, soil type, temperature, and atmospheric pressure.

Data and Resources

Data from the USArray Transportable Array (TA) and Superior Province Rifting Earthscope Experiment (SPREE) were obtained from the Incorporated Research Institutions for Seismology (IRIS) Data Management Center (<http://www.iris.edu>; last accessed October 2014). A sketch of the current TA vault configuration can be seen on the Array Network Facility's website (<http://anf.ucsd.edu/about>; last accessed May 2015). Soil data were obtained from the U.S. Department of Agriculture's Web Soil Survey (<http://websoilsurvey.nrcs.usda.gov>; last accessed November 2014). Frost-depth information was obtained from the Minnesota Department of Labor and Industry (<http://www.dli.mn.gov/CCLD/Codes.asp>; last accessed November 2014). Climate data were obtained from the Global Historical Climatology Network (<https://www.ncdc.noaa.gov/oa/climate/ghcn-daily>; last accessed May 2014; Menne *et al.*, 2012). Maps were created with Generic Mapping Tools (UTC; Wessel *et al.*, 2013). The ObsPy (Beyreuther *et al.*, 2010) and matplotlib (Hunter, 2007) Python packages were used to produce many of the plots.

Acknowledgments

The Superior Province Rifting Earthscope Experiment (SPREE) is supported by National Science Foundation (NSF) Grant EAR-0952345. The SPREE field experiment was supported by the Incorporated Research Institutions for Seismology Program for Array Seismic Studies of the Continental Lithosphere (IRIS PASSCAL) program.

We thank Michael Witek for sharing code that greatly expedited the calculation of power spectral densities for large volumes of data. Two anonymous reviewers provided detailed comments that helped improve the manuscript. Thanks are extended to Ian Williams and undergraduate students George Beduhn, Jeremy Mitchell, Willa Samuelson, Tim Sandmann, and Zach Weinfurter from the University of Wisconsin–River Falls for their assistance in demobilizing SPREE and collecting soil data.

References

- Aster, R. C., D. E. McNamara, and P. D. Bromirski (2008). Multidecadal climate-induced variability in microseisms, *Seismol. Res. Lett.* **79**, no. 2, 194–202.
- Beauduin, R., P. Lognonné, J. Montagner, S. Cacho, J. Karczewski, and M. Morand (1996). The effects of the atmospheric pressure changes on seismic signals or how to improve the quality of a station, *Bull. Seismol. Soc. Am.* **86**, no. 6, 1760–1769.
- Beyreuther, M., R. Barsch, L. Krischer, T. Megies, Y. Behr, and J. Wassermann (2010). Obspy: A Python toolbox for seismology, *Seismol. Res. Lett.* **81**, no. 3, 530–533.
- Bormann, P. (Editor) (2009). *New Manual of Seismological Observatory Practice*, GeoForschungsZentrum, Potsdam, Germany.
- Chapman, S., and R. S. Lindzen (1970). *Atmospheric Tides: Thermal and Gravitational*, Vol. 15, Springer, Dordrecht, The Netherlands.
- Custódio, S., N. A. Dias, B. Caldeira, F. Carrilho, S. Carvalho, C. Corela, J. Díaz, J. Narciso, G. Madureira, L. Matias, *et al.* (2014). Ambient noise recorded by a dense broadband seismic deployment in western Iberia, *Bull. Seismol. Soc. Am.* **104**, no. 6, 2985–3007.
- Dai, A., and C. Deser (1999). Diurnal and semidiurnal variations in global surface wind and divergence fields, *J. Geophys. Res.* **104**, no. D24, 31,109–31,125.
- Dai, A., and J. Wang (1999). Diurnal and semidiurnal tides in global surface pressure fields, *J. Atmos. Sci.* **56**, no. 22, 3874–3891.
- De Angelis, S., and P. Bodin (2012). Watching the wind: Seismic data contamination at long periods due to atmospheric pressure-field-induced tilting, *Bull. Seismol. Soc. Am.* **102**, no. 3, 1255–1265.
- Ebeling, C. W. (2012). Inferring ocean storm characteristics from ambient seismic noise: A historical perspective, *Adv. Geophys.* **53**, 1–34.
- Farouki, O. T. (1981). Thermal properties of soils, *Tech. Rept. 81-1*, U.S. Army Cold Regions Research and Engineering Laboratory.
- Given, H. K. (1990). Variations in broadband seismic noise at IRIS/IDA stations in the USSR with implications for event detection, *Bull. Seismol. Soc. Am.* **80**, no. 6B, 2072–2088.
- Gupta, S., and W. Larson (1979). Estimating soil water retention characteristics from particle size distribution, organic matter percent, and bulk density, *Water Resour. Res.* **15**, no. 6, 1633–1635.
- Hanka, W. (2009). Which parameters influence the very long period performance of a seismological station?: Examples from the GEOFON network, ftp://ftp.gfz-potsdam.de/home/st/jaeckl/bb_stations/which%20parameters.html (last accessed May 2015).
- Hayashi, M., G. van der Kamp, and R. Schmidt (2003). Focused infiltration of snowmelt water in partially frozen soil under small depressions, *J. Hydrol.* **270**, no. 3, 214–229.
- Herron, T., I. Tolstoy, and D. Kraft (1969). Atmospheric pressure background fluctuations in the mesoscale range, *J. Geophys. Res.* **74**, no. 6, 1321–1329.
- Holcomb, L. G., and C. R. Hutt (1992). An evaluation of installation methods for STS-1 seismometers, *U.S. Depart. Interior Geol. Surv. Open-File Rept.* 92-302.
- Hunter, J. D. (2007). Matplotlib: A 2D graphics environment, *Comput. Sci. Eng.* **9**, no. 3, 90–95.
- Hutt, C. R., and A. Ringler (2009). A summary of STS-2 low-noise installation methods tested at the USGS Albuquerque Seismological Laboratory, <http://bnordgren.org/seismo/STS-2%20Installation%20Methods.pdf> (last accessed May 2015).
- Koper, K. D., and R. Burlacu (2015). The fine structure of double-frequency microseisms recorded by seismometers in North America, *J. Geophys. Res.* **120**, no. 3, 1677–1691.
- Kristeková, M., J. Kristek, and P. Moczo (2009). Time-frequency misfit and goodness-of-fit criteria for quantitative comparison of time signals, *Geophys. J. Int.* **178**, no. 2, 813–825, doi: 10.1111/j.1365-246X.2009.04177.x.
- Longuet-Higgins, M. S. (1950). A theory of the origin of microseisms, *Phil. Trans. Roy. Soc. Lond.* **243**, no. 857, 1–35.
- McGinnis, L., K. Nakao, and C. Clark (1973). Geophysical identification of frozen and unfrozen ground, Antarctica, *Proc. 2nd International*

- Conference on Permafrost*, Yakutsk, Russia, 13–28 July 1973, 136–146.
- McNamara, D. E., and R. P. Buland (2004). Ambient noise levels in the continental United States, *Bull. Seismol. Soc. Am.* **94**, no. 4, 1517–1527.
- Menne, M. J., I. Durre, R. S. Vose, B. E. Gleason, and T. G. Houston (2012). An overview of the Global Historical Climatology Network-Daily Database, *J. Atmos. Ocean. Technol.* **29**, no. 7, 897–910.
- Nishida, K. (2013). Earth's background free oscillations, *Annu. Rev. Earth Planet. Sci.* **41**, 719–740.
- Peck, A. J. (1960). The water table as affected by atmospheric pressure, *J. Geophys. Res.* **65**, no. 8, 2383–2388, doi: [10.1029/JZ065i008p02383](https://doi.org/10.1029/JZ065i008p02383).
- Peterson, J. (1993). Observations and modeling of seismic background noise, *Tech. Rept. 93-322, U.S. Geol. Surv. Open-File Rept. 93-322*.
- Press, F. (1966). Seismic velocities, in *Handbook of Physical Constants*, S. P. Clark (Editor), Geol. Soc. Am. Memoir, Vol. 97, 195–218.
- Ray, R., and R. Ponte (2003). Barometric tides from ECMWF operational analyses, *Annales Geophysicae* **21**, no. 8, 1897–1910.
- Rhie, J., and B. Romanowicz (2004). Excitation of Earth's continuous free oscillations by atmosphere–ocean–seafloor coupling, *Nature* **431**, no. 7008, 552–556.
- Ringdal, F., and H. Bungum (1977). Noise level variation at NORSAR and its effect on detectability, *Bull. Seismol. Soc. Am.* **67**, no. 2, 479–492.
- Ringler, A. T., and C. R. Hutt (2010). Self-noise models of seismic instruments, *Seismol. Res. Lett.* **81**, no. 6, 972–983, doi: [10.1785/gssrl.81.6.972](https://doi.org/10.1785/gssrl.81.6.972).
- Shapiro, N. M., M. Campillo, L. Stehly, and M. H. Ritzwoller (2005). High-resolution surface-wave tomography from ambient seismic noise, *Science* **307**, no. 5715, 1615–1618.
- Sorrells, G. G. (1971). A preliminary investigation into the relationship between long-period seismic noise and local fluctuations in the atmospheric pressure field, *Geophys. J. Int.* **26**, nos. 1/4, 71–82.
- Spang, F. A. (2002). Considering barometric pressure in groundwater flow investigations, *Water Resour. Res.* **38**, no. 6, 14-1–14-18, doi: [10.1029/2001WR000701](https://doi.org/10.1029/2001WR000701).
- Stein, S., S. van der Lee, D. Jurdy, C. Stein, D. Wiens, M. Wyssession, J. Revenaugh, A. Frederiksen, F. Darbyshire, T. Bollmann, et al. (2011). Learning from failure: The SPREE mid-continent rift experiment, *GSA Today* **21**, no. 9, 5–7.
- Stutzmann, E., G. Roult, and L. Astiz (2000). GEOSCOPE station noise levels, *Bull. Seismol. Soc. Am.* **90**, no. 3, 690–701, doi: [10.1785/0119990025](https://doi.org/10.1785/0119990025).
- Sufri, O., K. D. Koper, R. Burlacu, and B. de Foy (2014). Microseisms from superstorm Sandy, special issue on USArray science, *Earth Planet. Sci. Lett.* **402**, 324–336.
- Tsuda, T., and S. Kato (1989). Diurnal non-migrating tides excited by a differential heating due to land-sea distribution, *J. Meteorol. Soc. Japan* **67**, no. 1, 43–55.
- Usher, M., C. Guralp, and R. Burch (1978). The design of miniature wide-band seismometers, *Geophys. J. Int.* **55**, no. 3, 605–613.
- van der Lee, S., E. Wolin, T. Bollmann, and K. Tekverk (2013). Crust and mantle structure of a closed rift system from the Superior Province Rifting Earthscope Experiment (SPREE), *AGU Fall Meeting Abstracts*, San Francisco, California, 9–13 December 2013, Vol. 1, 1 pp.
- Vila, J. (1998). The broadband seismic station CAD (Tunel del Cadi, eastern Pyrenees): Site characteristics and background noise, *Bull. Seismol. Soc. Am.* **88**, no. 1, 297–303.
- Vila, J., and R. Macià (2002). The broadband seismic station CADI (Tunel del Cadi, eastern Pyrenees), part II: Long-period variations of background noise, *Bull. Seismol. Soc. Am.* **92**, no. 8, 3329–3334.
- Webb, S. C. (2007). The Earth's 'hum' is driven by ocean waves over the continental shelves, *Nature* **445**, no. 7129, 754–756.
- Wessel, P., W. H. Smith, R. Scharroo, J. Luis, and F. Wobbe (2013). Generic Mapping Tools: Improved version released, *Eos Trans. AGU* **94**, no. 45, 409–410.
- Whitmeyer, S. J., and K. E. Karlstrom (2007). Tectonic model for the Proterozoic growth of North America, *Geosphere* **3**, no. 4, 220–259.
- Wielandt, E., and G. Streckeisen (1982). The leaf-spring seismometer: Design and performance, *Bull. Seismol. Soc. Am.* **72**, no. 6A, 2349–2367.
- Wilson, D., J. Leon, R. Aster, J. Ni, J. Schlue, S. Grand, S. Semken, S. Baldrige, and W. Gao (2002). Broadband seismic background noise at temporary seismic stations observed on a regional scale in the southwestern United States, *Bull. Seismol. Soc. Am.* **92**, no. 8, 3335–3342, doi: [10.1785/0120010234](https://doi.org/10.1785/0120010234).
- Withers, M. M., R. C. Aster, C. J. Young, and E. P. Chael (1996). High-frequency analysis of seismic background noise as a function of wind speed and shallow depth, *Bull. Seismol. Soc. Am.* **86**, no. 5, 1507–1515.
- Woodward, R., R. Busby, K. Hafner, J. Gridley, A. Schultz, A. Frassetto, and D. Simpson (2013). EarthScope's USArray: A decade of observations and results, *AGU Fall Meeting Abstracts*, San Francisco, California, 9–13 December 2013, Vol. 1, 2.
- Young, C. J., E. P. Chael, D. A. Zagar, and J. A. Carter (1994). Variations in noise and signal levels in a pair of deep boreholes near Amarillo, Texas, *Bull. Seismol. Soc. Am.* **84**, no. 5, 1593–1607.
- Zürn, W., J. Exss, H. Steffen, C. Kroner, T. Jahr, and M. Westerhaus (2007). On reduction of long-period horizontal seismic noise using local barometric pressure, *Geophys. J. Int.* **171**, no. 2, 780–796.

Department of Earth and Planetary Sciences
Northwestern University
2145 Sheridan Road
Room F379
Evanston, Illinois 60208
emilyw@earth.northwestern.edu
(E.W., S.v., T.A.B., S.S.)

Department of Earth and Planetary Sciences
Washington University in Saint Louis
Campus Box 1169
One Brookings Drive
St. Louis, Missouri 63130
(D.A.W., M.E.W.)

Department of Earth Sciences
University of Minnesota
310 Pillsbury Drive SE
Minneapolis, Minnesota 55455
(J.R.)

Centre de Recherche GEOTOP
Université du Québec à Montréal CP 8888, succ. Centre-Ville
Montréal, Québec
Canada H3C 3P8
(F.A.D.)

Department of Geological Sciences
University of Manitoba
240 Wallace Building
125 Dysart Road
Winnipeg, MB
Canada R3T 2N2
(A.W.F.)

Manuscript received 9 February 2015;
Published Online 8 September 2015